High energy evolution for Gribov-Zwanziger confinement: Solution to the equation

E. Gotsman,[1,*] Yu. P. Ivanov,[2,3,†] and E. Levin[1,3,‡]

[1]*Department of Particle Physics, School of Physics and Astronomy, Raymond and Beverly Sackler Faculty of Exact Science, Tel Aviv University, Tel Aviv 69978, Israel*
[2]*Joint Institute for Nuclear Research (JINR), Dubna, 141980 Moscow Region, Russia*
[3]*Departamento de Física, Universidad Técnica Federico Santa María and Centro Científico Tecnológico de Valparaíso, Casilla 110-V, Valparaiso, Chile*

(Received 4 January 2021; accepted 21 April 2021; published 19 May 2021)

In this paper, we solve the new evolution equation for high energy scattering amplitude that stems from the Gribov-Zwanziger approach to the confinement of quarks and gluons. We found that (1) the energy dependence of the scattering amplitude turns out to be the same as for QCD Balitsky, Fadin, Kuraev and Lipatov (BFKL) evolution, (2) the spectrum of the new equation does not depend on the details of the Gribov-Zwanzinger approach, and (3) all eigenfunctions coincide with the eigenfunctions of the QCD BFKL equation at large transverse momenta $\kappa \geq 1$. The numerical calculations show that there exist no new eigenvalues with the eigenfunctions which decrease faster than solutions of the QCD BFKL equation at large transverse momenta. The structure of the gluon propagator in the Gribov-Zwanziger approach, that stems from the lattice QCD and from the theoretical evaluation, results in the exponential suppression of the eigenfunctions at long distances and in the resolution of the difficulties, which the color glass condensate and some other approaches, based on perturbative QCD, face at large impact parameters. We can conclude that the confinement of quark and gluons, at least in the form of the Gribov-Zwanziger approach, does not influence on the scattering amplitude except for solving the long-standing theoretical problem of its behavior at large impact parameters.

DOI: 10.1103/PhysRevD.103.096017

I. INTRODUCTION

It is well known that perturbative QCD suffers a fundamental problem: the scattering amplitude decreases at large impact parameters (b) as a power of b. Such behavior contradicts the Froissart theorem [1], and, hence, perturbative QCD cannot lead to an effective theory at high energy. In particular, the color glass condensate/saturation approach (see Ref. [2] for a review), which is based on perturbative QCD, is confronted by this problem [3,4]. At large b, the scattering amplitude is small, and therefore only the linear Balitsky, Fadin, Kuraev, and Lipatov (BFKL) equation [5] describes the scattering amplitude in perturbative QCD. It is known that the eigenfunction of this equation (the scattering amplitude of two dipoles with sizes r and R) has the following form [6]:

$$\phi_\gamma(\boldsymbol{r},\boldsymbol{R},\boldsymbol{b}) = \left(\frac{r^2R^2}{(\boldsymbol{b}+\frac{1}{2}(\boldsymbol{r}-\boldsymbol{R}))^2(\boldsymbol{b}-\frac{1}{2}(\boldsymbol{r}-\boldsymbol{R}))^2}\right)^\gamma \xrightarrow{b\gg r,R} \left(\frac{r^2R^2}{b^4}\right)^\gamma. \tag{1}$$

One can see that $\phi_\gamma(\boldsymbol{r},\boldsymbol{R},\boldsymbol{b})$ at large impact parameter b decreases as a power of b. In particular, such a decrease leads to the growth of the radius of interaction as a power of the energy [3,4], resulting in the violation of Froissart theorem. Since it was proven in Ref. [6] that the eigenfunction of any kernel with conformal symmetry has the form of Eq. (1), we can only change the large-b behavior by introducing a new dimensional scale in the kernel of the equation. A variety of ideas to overcome this problem have been suggested in Refs. [4,7–26]. In our previous paper [27], we used the Gribov-Zwanziger approach [28–38] for the confinement of quarks and gluons to fix this nonperturbative scale. We derived the generalized BFKL evolution equation, which incorporates this new dimensional scale, and demonstrated that this equation leads to

*Deceased.
†yuri.ivanov@usm.cl
‡leving@tauex.tau.ac.il, eugeny.levin@usm.cl

the exponential decrease of the scattering amplitude at large b. We will discuss both the equation and large-b behavior of the solution in the next section, which has a review character.

In this paper, we find the solution to this new equation. In Sec. III, we consider the general properties of the spectrum and eigenfunctions, which follow from an analytical approach. In particular, we prove that the eigenfunctions of Eq. (1) describe the eigenfunctions of the new equation at short distances $r \ll R$. In Sec. IV, we concentrate our efforts on the numerical solution of the equation. We show that all eigenvalues of the new equation, that generate the power energy increase of the scattering amplitude, coincide with the massless BFKL eigenvalues. However, the eigenfunctions have quite a different behavior in comparison with the eigenfunction of the massless BFKL equation, and they crucially depend on the input from Gribov-Zwanziger confinement approach. Finally, in Sec. V, we discuss our results and future prospects.

II. BFKL EVOLUTION EQUATION FOR GRIBOV-ZWANZIGER CONFINEMENT: A RECAP

A. Gribov-Zwanziger confinement: Gluon propagator

As we have alluded, it was proved [6] that eigenfunctions of Eq. (1) have the same form for all kernels with conformal symmetries. Hence, we have to modify the kernel of the BFKL equation introducing a new dimensional scale of the nonperturbative origin. In other words, we need an approach which models the confinement of quarks and gluons. Among numerous approaches to confinement, the one proposed by Gribov, [28–38] has special advantages, which makes it most suitable for discussion of the BFKL equation in the framework of this hypotheses. First, it is based on the existence of Gribov copies [28]—multiple solutions of the gauge-fixing conditions, which are the principle properties of nonperturbative QCD. Second, the main ingredient is the modified gluon propagator, which can be easily included in the BFKL type of equations. Third, in Ref. [24] (see also Ref. [39]), it is demonstrated that the Gribov gluon propagator originates naturally from the topological structure of nonperturbative QCD in the form

$$G(q) = \frac{1}{q^2 + \frac{\chi_{\rm top}}{q^2}} = \frac{q^2}{q^4 + \mu^4}, \tag{2}$$

where $\chi_{\rm top} = \mu^4$ is the topological susceptibility of QCD, which is related to the η' mass by the Witten-Veneziano relation [40,41]. This allows us to obtain the principal nonperturbative dimensional scale, directly from the experimental data.

However, it is shown in Ref. [27] that the propagator of Eq. (2), which vanishes at $q = 0$, does not lead to the exponential suppression of the scattering amplitude at large impact parameters (b). Fortunately, the lattice calculation of the gluon propagator generates the gluon propagator with $G(q = 0) \neq 0$ (see Refs. [42–44] and references therein), in explicit contradiction with Eq. (2).

In Refs. [43–59],[1] it is shown that $G(q = 0) \neq 0$ is a general feature of nonperturbative approaches and that Gribov's copies lead to the gluon propagator which is final at $q \to 0$. In this paper, we parametrize the gluon propagator in the following form:

$$G(q) = \frac{q^2 + M_0^2}{(q^2 + M^2)^2 + \mu^4}, \tag{3}$$

We view this form as parametrization of the sum of Gribov's propagators of Eq. (2) with different values of μ, as has been discussed in Ref. [27]. We are aware that Eq. (3), which describes the lattice QCD data, is a simplified version of the refined Gribov-Zwanziger (RGZ) theoretical approaches that have been discussed in Refs. [43–59]. However, we believe that it is a good first approximation, which allows us to introduce two-dimensional parameters from confinement physics. In this paper, we call the gluon propagator of Eq. (3) the lattice QCD propagator or the RGZ propagator.

As we have mentioned, at high energies, q is a two-dimensional vector, which corresponds to transverse momentum carried by the gluon. Introducing

$$G^{\pm}(q) = \frac{1}{(q^2 + M^2) \pm i\mu^2}, \tag{4}$$

we can rewrite Eq. (3) in the form

$$\begin{aligned} G(q) &= \frac{1}{2}(G^+(q) + G^-(q)) + \frac{M_0^2 - M^2}{2i\mu^2}(G^+(q) - G^-(q)) \\ &= \frac{1}{\mu^2}(\mathrm{Re}G^+(\kappa) + (M_0^2 - M^2)\mathrm{Im}G^+(\kappa)) \\ &= \frac{1}{2}\left\{\left(1 + i\frac{M_0^2 - M^2}{\mu^2}\right)G^+(q) \right. \\ &\quad \left. + \left(1 - i\frac{M_0^2 - M^2}{\mu^2}\right)G^-(q)\right\} \\ &= \frac{1}{2\mu^2}\{(1 + im_0)G^+(\kappa) + (1 - im_0)G^-(\kappa)\}, \end{aligned} \tag{5}$$

where we use notations

$$\kappa = \frac{q^2}{\mu^2}, \quad \kappa' = \frac{q'^2}{\mu^2}, \quad E = -\frac{\omega}{\bar{\alpha}_S}, \quad \bar{\alpha}_S = \frac{\alpha_S N_c}{\pi}, \quad m = \frac{M^2}{\mu^2}, \quad m_0 = \frac{M_0^2 - M^2}{\mu^2}. \tag{6}$$

[1]This list of references is not complete. More details can be found in the reviews [37,45].

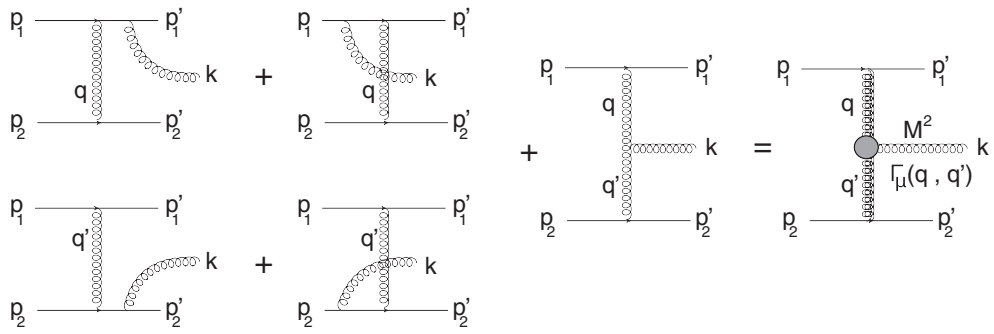

FIG. 1. The first Feynman diagrams with gluon emission, whose sum leads to $\Gamma_\nu(q,q')$ (Lipatov vertex is denoted by the gray blob).

It is worth it to mention that Eq. (6) introduces the dimensionless variables for our problem and sets the physical scale for the dimensionful quantities: μ^2.

B. BFKL equation in momentum representation

The BFKL equation for Gribov-Zwanziger gluon propagator has been derived in our previous paper [27], using the procedure that has been described in Ref. [22].

It has two parts: the gluon Reggeization and the emission of gluons. The first one has a general form [5],

$$\omega_G(q) = G^{-1}(q)\Sigma(q)$$
$$\text{with} \quad \Sigma(q) = \int \frac{d^2q'}{4\pi} G(\boldsymbol{q}')G(\boldsymbol{q}-\boldsymbol{q}'), \tag{7}$$

where $G(q)$ is given by Eq. (3). We will discuss the analytical expression for Eq. (7) below (see also Appendix A of Ref. [27]).

The emission kernel has been calculated in Ref. [27] using the decomposition of Eq. (2). Indeed, using this decomposition, we can treat the production of the gluon as the sum of two sets of the diagrams (see Fig. 1) with $\tilde{M}^2 = i\mu^2$ and with $\tilde{M}^2 = -i\mu^2$.

We sum the first diagrams of the gluon emission shown in Fig. 1 to find the vertex $\Gamma_\mu(q,q')$ for the kernel of the BFKL equation. It is easy to see that the sum shown in Fig. 1 leads to the Lipatov vertex that has the form [22]

$$\Gamma_\mu(q,q') = -q_\mu^\perp - q'^\perp_\mu + p_{1,\mu}\left(-G^{-1}(q)\frac{1}{p_1\cdot k} + \frac{p_2\cdot k}{p_1\cdot p_2}\right) - p_{2,\mu}\left(-G^{-1}(q')\frac{1}{p_2\cdot k} + \frac{p_1\cdot k}{p_1\cdot p_2}\right), \tag{8}$$

where $p_{1,\mu}$ and $p_{2,\mu}$ are the momenta of incoming particles (see Fig. 1 for all notations).

Using Eqs. (7) and (8), the BFKL equation for Gribov-Zwanziger confinement takes the form (for $\boldsymbol{Q}_T = 0$[2]):

$$\omega\phi(\omega,q) = -2\omega_G(q)\phi(\omega,q) + \bar{\alpha}_S\int\frac{d^2q'}{\pi}G(\boldsymbol{q}-\boldsymbol{q}')\phi(\omega,q'). \tag{9}$$

This equation looks similar to the BFKL equation for a massive gluon [22] in the non-Abelian Yang-Mills theories with a Higgs particle, which is responsible for mass generation. However, we do not have a contact term in Eq. (9). As we have discussed in Ref. [27], the absence of a contact term in our equation is a direct indication that Gribov-Zwanziger confinement does not lead to a massive gluon.

Assuming that $\phi(q)$ depends only on $|\boldsymbol{q}|$, we can integrate the emission kernel over the angle, and in terms of the variable of Eq. (6), Eq. (9) takes the form

$$E\phi(\kappa) = \underbrace{T(\kappa)\phi(\kappa)}_{\text{kinetic energy}} - \underbrace{\int d\kappa' K(\kappa,\kappa')\phi(\kappa')}_{\text{emission kernel}} \tag{10a}$$

$$= -T(\kappa)\phi(\kappa) - \int d\kappa' K(\kappa,\kappa')\left\{\phi(\kappa') - \frac{G(\kappa')}{G(\kappa)}\phi(\kappa)\right\}, \tag{10b}$$

where

$$T(\kappa) = \frac{1}{4}G^{-1}(\kappa)\{\mathrm{Re}(\tilde{m}_0^2 I_1(\tilde{m},\kappa)) + (1+m_0^2)I_2(m,\kappa)\}, \tag{11a}$$

$$I_1(\tilde{m},\kappa) = \frac{2}{\sqrt{\kappa(\kappa+4\tilde{m})}}\ln\left(\frac{\sqrt{\kappa}+\sqrt{\kappa+4\tilde{m}}}{-\sqrt{\kappa}+\sqrt{\kappa+4\tilde{m}}}\right), \tag{11b}$$

$$I_2(m,\kappa) = -\frac{1}{\sqrt{4m\kappa+\kappa^2-4}} \times \ln\left(\frac{\kappa+2m-\sqrt{4m\kappa+\kappa^2-4}}{\kappa+2m+\sqrt{4m\kappa+\kappa^2-4}}\right), \tag{11c}$$

[2] $\boldsymbol{Q}_T$ is the momentum transferred by the BFKL Pomeron, a conjugate variable to the impact parameter.

$$K(\kappa,\kappa') = \mathrm{Re}\left\{\frac{\tilde{m}_0}{\sqrt{2\tilde{m}(\kappa+\kappa')+\tilde{m}^2+(\kappa-\kappa')^2}}\right\}, \quad (11d)$$

$$G(\kappa) = \frac{\kappa+m+m_0}{(\kappa+m)^2+1}, \quad (11e)$$

$$\tilde{m} = m+i, \quad \tilde{m}_0 = 1+im_0. \quad (11f)$$

In Eq. (10a)–Eq. (11e), we use the variables which are given in Eq. (6). As has been mentioned, Eq. (6) sets the scale for the dimensionful observables: the Gribov mass μ^2 [see Eqs. (2) and (3)]. In Eq. (11f), we introduce new variables only to rewrite Eq. (10b) in the most compact form.

III. BASICS OF THE SPECTRUM FOR THE MASTER EQUATION

A. Equation for the eigenfunctions of the massless BFKL equation

As has been mentioned, the eigenfunctions of the massless BFKL equation

$$\phi_{\mathrm{BFKL}}(\kappa;\gamma) = \kappa^{\gamma-1} \quad \text{with} \quad \gamma = \frac{1}{2}+i\nu \quad (12)$$

form the complete and orthogonal set of functions. Hence, we can expect that the solution to the master equation can be written as the sum over these functions. For this reason, we find it instructive to consider how the emission kernel of our master equation [see Eq. (10a)] acts on the eigenfunctions of Eq. (12),

$$\int d\kappa' K(\kappa,\kappa')\kappa'^{\gamma-1} - \chi(\gamma)\kappa^{\gamma-1} = \int_0^\infty d\kappa' \mathrm{Re}\left\{\frac{\tilde{m}_0}{\sqrt{2\tilde{m}(\kappa+\kappa')+\tilde{m}^2+(\kappa-\kappa')^2}}\right\}\kappa'^{\gamma-1} - \chi(\gamma)\kappa^{\gamma-1} \quad (13a)$$

$$\to \kappa^{\gamma-1}\left\{\int_0^1 dt(t^{\gamma-1}-1)\mathrm{Re}\left(-\frac{1}{\sqrt{(1-t)^2}}+\frac{\tilde{m}_0}{\sqrt{(\tilde{m}/\kappa)^2+2(t+1)\tilde{m}/\kappa+(1-t)^2}}\right)\right.$$
$$\left. + \int_0^1 dt(t^{-\gamma}-1)\mathrm{Re}\left(-\frac{1}{\sqrt{(1-t)^2}}+\frac{\tilde{m}_0}{\sqrt{(t\tilde{m}/\kappa)^2+2(t+1)t\tilde{m}/\kappa+(1-t)^2}}\right)\right\} \quad (13b)$$

$$\equiv \kappa^{\gamma-1}P(\kappa,\gamma), \quad (13c)$$

where the kernel of massless BFKL $\chi(\gamma)$ has the form [5]

$$\chi(\gamma) = \psi(1-\gamma)+\psi(\gamma)-2\psi(1) = \psi\left(\frac{1}{2}+i\nu\right)+\psi\left(\frac{1}{2}-i\nu\right)-2\psi(1), \quad (14)$$

where $\psi(z)$ is the Euler ψ-function (formula (8.36) of Ref. [60]).

In Eq. (13b), the region of integration over κ' is divided in two: $\kappa' \le \kappa$ and $\kappa' \ge \kappa$. In the first region, the new variable is introduced $t = \kappa'/\kappa$, while in the second, the new variable is $t = \kappa/\kappa'$. In this way, we have both t's in the region (0,1). In addition, we subtracted in Eq. (13b) (terms with 1 in the numerators of the equation) the contribution from the Regge trajectory [see Eq. (7)].

Using formula (3.211) of Ref. [60], we can express these integral over t through the Appel F_1 function [see Ref. [60], formulas (9.180)–(9.184)]:

$$P(\kappa,\gamma)+\chi(\gamma) = \mathrm{Re}\left\{\tilde{m}_0\left[\frac{\kappa}{\gamma(\kappa+\tilde{m})}F_1\left(\gamma;\frac{1}{2},\frac{1}{2};\gamma+1;\frac{\kappa}{\kappa-\tilde{m}-2\sqrt{-\kappa\tilde{m}}},\frac{\kappa}{\kappa-\tilde{m}+2\sqrt{-\kappa\tilde{m}}}\right)\right.\right.$$
$$-\frac{\sqrt{4\kappa^3+\tilde{m}(3\kappa+\tilde{m})^2}}{(\gamma-1)(\kappa+\tilde{m})\sqrt{4\kappa+\tilde{m}}}F_1\left(1-\gamma;\frac{1}{2},\frac{1}{2};2-\gamma;\frac{(\kappa+\tilde{m})^2}{\kappa-\tilde{m}-2\sqrt{-\kappa\tilde{m}}},\frac{(\kappa+\tilde{m})^2}{\kappa-\tilde{m}+2\sqrt{-\kappa\tilde{m}}}\right)$$
$$\left.\left.+\ln\left(\frac{2}{1+\sqrt{1+4\kappa/\tilde{m}}}\right)-\frac{\kappa}{\kappa+\tilde{m}}\ln\left(\frac{1}{2\kappa}\left[\frac{\kappa+\tilde{m}}{\tilde{m}}\sqrt{\tilde{m}(4\kappa+\tilde{m})}+3\kappa+\tilde{m}\right]\right)\right]\right\}. \quad (15)$$

From Eqs. (13b) and (15) [see also Fig. 2(a)], we can see that $P(\kappa,\gamma)$ is rather small and decreases at large positive $l = \ln\kappa$.

Since in Eq. (13b) we subtract the Reggeization term, we have redefined the kinetic term in Eq. (10a), subtracting from $T(\kappa)$ of Eq. (11a) function $L(\kappa)$, which is

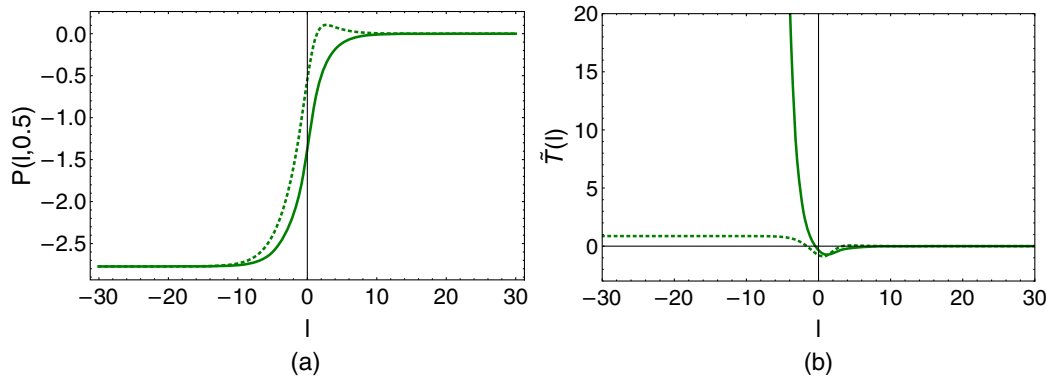

FIG. 2. Functions $P(\kappa = e^l, \gamma = 0.5)$ [Fig. 2(a)] and $\tilde{T}(e^l)$ [Fig. 2(b)] vs l. In these figures, the solid lines describe the case $m = m_0 = 0$, while the dotted ones correspond to $m = 1.27, m_0 = 3.76$, which follows from the lattice QCD estimates [42].

$$L(\kappa) = \int_0^1 dtt \frac{\tilde{m}_0}{\sqrt{(t\tilde{m}_0/\kappa)^2 + 2(t+1)t\tilde{m}_0/\kappa + (1-t)^2}} + \int_0^1 dt \frac{\tilde{m}_0}{\sqrt{(\tilde{m}_0/\kappa)^2 + 2(t+1)\tilde{m}_0/\kappa + (1-t)^2}}$$
$$= \tilde{m}_0 \ln\left(\frac{1+\sqrt{1+4\kappa/\tilde{m}}}{2}\right) + \frac{\kappa\tilde{m}_0}{\kappa+\tilde{m}} \ln\left(\frac{1}{2\kappa}\left[\frac{\kappa+\tilde{m}}{\tilde{m}}\sqrt{\tilde{m}(4\kappa+\tilde{m})} + 3\kappa + \tilde{m}\right]\right). \quad (16)$$

We denote

$$\tilde{T}(l) = T(e^l) - \mathrm{Re}L(e^l). \quad (17)$$

$\tilde{T}(l)$ is plotted in Fig. 2(b).

Using function $P(l,\gamma)$ and $\tilde{T}(l)$, we see that our equation for the function $e^{(\gamma-1)l}$ has the form

$$(E + \chi(\gamma))e^{(\gamma-1)l} = e^{(\gamma-1)l}(P(l,\gamma) - \tilde{T}(l)) = e^{(\gamma-1)l}\tilde{P}(l,\gamma). \quad (18)$$

In Fig. 3, we plot

$$E(\nu) = -\chi(\nu) + \tilde{P}(l,\nu), \quad (19)$$

fixing $\gamma = \frac{1}{2} + i\nu$. Figure 3(a) gives Eq. (19) for $m = m_0 = 0$, which corresponds to the Gribov gluon propagator, while in Fig. 3(b), the energy is plotted for the lattice QCD gluon propagator with $m = 1.27$ and $m_0 = 3.76$ [42].

One can see that the wave functions of the massless BFKL show up as the eigenfunctions of the master equation in the kinematic region of large $l = \ln\kappa \gg 1$. Generally speaking, it means that the eigenvalues of Eq. (10a) could be (1) the same as the massless one or (2) selected out due to behavior at small κ, leading to the set of the eigenvalues, which is more restricted than the massless BFKL one. In addition, of course, could be some discrete states, whose wave functions decrease more steeply than $\kappa^{\gamma-1}$ at large

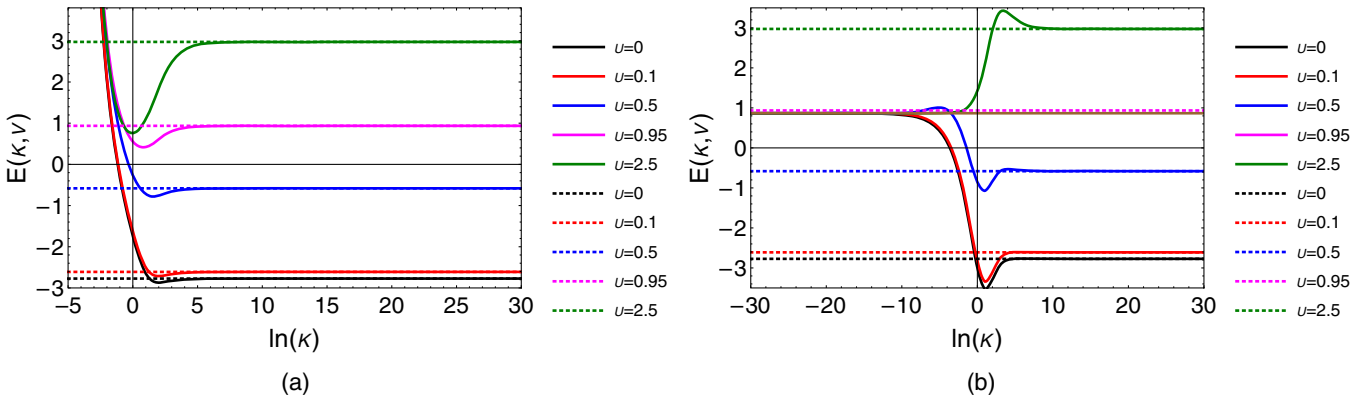

FIG. 3. The dependence of the energies of the master equation [see Eq. (10a)] versus $l = \ln\kappa$ for the eigenfunctions of Eq. (12) with different values of $\gamma\frac{1}{2} + i\nu$. The dotted lines describe the eigenvalues of the massless BFKL equation. Figure 3(a) describes the energies for the Gribov gluon propagator [see Eq. (2)], while Fig. 3(b) corresponds to the gluon propagator of Eq. (3) with $m = 1.27$ and $m_0 = 3.76$, which follows from the lattice QCD estimates [42]. The brown line in Fig. 3(b) shows $E = T(\kappa = 0)$.

values of κ. From the numerical solution (see below), we see that there is no selection and all energies of the massless BFKL equations occur as the eigenvalues of the master equation. We can understand this, since all BFKL eigenvalues are doubly degenerate. Indeed, the eigenvalues of the massless BFKL equation do not depend on the sign of ν [see Eq. (14)]. At $l < 0$, we expect the eigenfunction of the massive BFKL equation to be constant. Replacing this behavior by the boundary condition $\phi(l = 0; \nu) =$ Const, we see that we can satisfy this boundary condition choosing $\phi(l) = C_1\phi_{\rm BFKL}(l, \nu) + C_2\phi_{\rm BFKL}(l, -\nu) = \sin(l\nu + \varphi)$, where φ is the phase. Hence, we do not bring any selection with this procedure.

However, the eigenfunctions of the massless BFKL equation appear the eigenfunctions of Eq. (18) also for $\kappa \ll 1$ ($l = \ln\kappa \ll -1$) [see Fig. 3(b)], but only for the case of $m \neq 0$ and $m_0 \neq 0$ with the eigenvalue $E_0 = T(\kappa = 0) = 0.866$ for any value of ν [brown line in Fig. 3(b)]. The independence of ν means that the eigenvalue ω_0 is infinitely degenerate. Figure 2(c) shows that in Eq. (19) $E(\nu) = \{-\chi(\nu) + P(l, \gamma)\} - \tilde{T}(l)$ the term in $\{\ldots\}$ vanishes at $l < 0$ [see Fig. 2(c)], while $\tilde{T}(l)$ approaches a constant [see Fig. 2(b)].

In principle, such solutions could be rejected for the master equation if the behavior at small κ cannot be matched with the behavior at large κ. However, it looks very unlikely. Indeed, any function of the type $\phi(\kappa) = P_n(2\kappa - 1)\Theta(1 - \kappa)$, where $P_n(z)$ is the Legendre polynomial [see Ref. [60], formulas (8.91)], is orthogonal to $\phi(\kappa) =$ Const at $l < 0$ (for $n > 1$) and satisfies Eq. (18). The numerical calculations, which we will discuss below, confirm that $E = E_0$ appears as the eigenvalue of the generalization of the BFKL equation [see Eq. (10a)].

B. General features of the spectrum

Following the general pattern of Ref. [22], we can rewrite Eq. (10a) in the coordinate space, introducing

$$\Psi(r) = \int \frac{d^2q_T}{(2\pi)^2} e^{ir\cdot q_T}\phi(q_T). \tag{20}$$

The equation takes the form

$$E\Psi(r) = \mathcal{H}\Psi(r) \tag{21}$$

with

$$\mathcal{H} = \underbrace{T(\hat{\kappa})}_{\text{kinetic energy}} - \underbrace{U(r)}_{\text{potential energy}} = T(\hat{\kappa}) - G(r), \tag{22}$$

where $\hat{\kappa} = -\nabla_r^2$ is the momentum operator and $G(r)$ is equal to

$$G(r) = \int \frac{d^2q_T}{(2\pi)^2} e^{ir\cdot q_T} G(q_T) = \tilde{m}_0 K_0(\sqrt{\tilde{m}}r) + \tilde{m}_0{}^* K_0(\sqrt{\tilde{m}^*}r) \xrightarrow{r\gg m} \mathrm{Re}\left\{\frac{\tilde{m}_0}{\tilde{m}^{1/4}}\sqrt{\frac{\pi}{2r}}e^{-\sqrt{\tilde{m}}r}\right\}. \tag{23}$$

For large r, $G(r)$ exponentially decreases as one can see from Eq. (23). Hence, at large r, Eq. (21) takes the form

$$E\Psi(r) = T(\hat{\kappa})\Psi(r) \tag{24}$$

with the eigenfunctions that have the following form:

$$\phi(\boldsymbol{r}) \sim e^{i\sqrt{\kappa^2}r}, \quad \kappa^2 > 0; \qquad \phi(\boldsymbol{r}) \sim e^{-\sqrt{-\kappa^2}r}, \quad \kappa^2 < 0. \tag{25}$$

Denoting the large asymptotic behavior of the eigenfunction as $\Psi(r) \overset{r\gg 1/\mu}{\to} \exp(-\sqrt{a}r)$, we see that the energy is equal to

$$E = T(-a). \tag{26}$$

On the other hand, in the region of small r, Eq. (22) reduces to the massless QCD BFKL equation (see the previous section and Refs. [5,6])

$$E\Psi(r)\Psi(r) = \mathcal{H}_0\Psi(r), \tag{27}$$

where [6]

$$\mathcal{H}_0 = \ln p^2 + \ln|r|^2 - 2\psi(1). \tag{28}$$

The eigenfunctions of Eq. (27) are $\Psi(r) = r^{2(1-\gamma)}$, and the eigenvalues of Eq. (27) can be parametrized as a function of γ [see Eq. (14)]. Therefore, for $r \to 0$ we have the eigenvalue which is equal to

$$E = \chi(\gamma). \tag{29}$$

From Eqs. (26) and (29), we can conclude that the values of a and γ are correlated, since

$$E = \chi(\gamma) = T(-a). \tag{30}$$

Based on Eq. (29) (see also the previous section), we expect that the minimum eigenvalue is equal to $\chi(\frac{1}{2}) = -4\ln 2$. From Fig. 4, we can see that Eq. (30) is violated. For Gribov's propagator of Eq. (2), $T(\kappa)$ is positive for all values of $-\infty < \kappa < +\infty$. For the gluon propagator that describes the lattice QCD estimates ($m = 1.27$ and $m_0 = 3.76$), we can see from Fig. 4(b) that $T(\kappa)$ is negative at $\kappa < 0$, and therefore, Eq. (30) can be satisfied.

On the other hand, the estimates of Eq. (26) contradict the result of Ref. [27] that the eigenfunction of the master

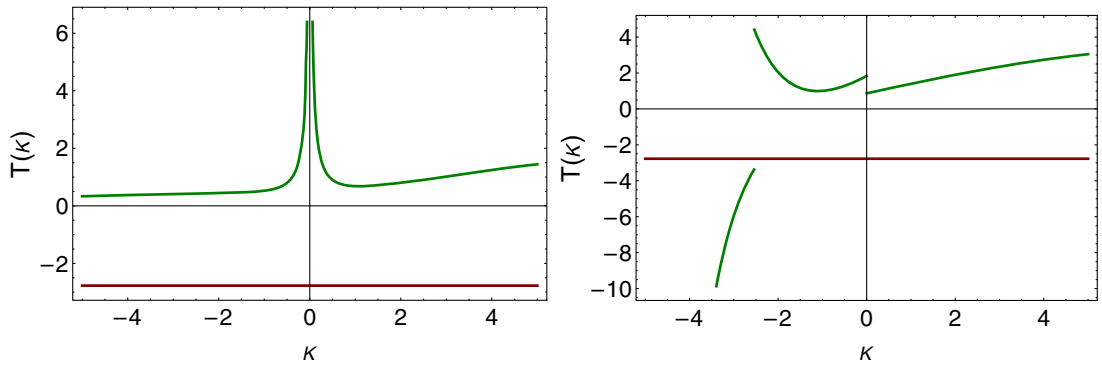

FIG. 4. $T(\kappa)$ vs κ for Gribov's propagator of Eq. (2) ($m = m_0 = 0$) and for the gluon propagator that describes the lattice QCD estimates ($m = 1.27$ and $m_0 = 3.76$). The red line shows $E = -4\ln 2$, which is the ground state for the massless BFKL equation.

equation with the Gribov gluon propagator exhibits the powerlike decrease at long distances. We believe that a resolution of this inconsistency is intimately related to the definition of $\Psi(r)$. In particular, instead of Eq. (20), we suggest introducing the following transform to the coordinate space. First, we introduce a new $\tilde{\phi}(\kappa) = G^{-1}(\kappa)\phi(\kappa)$. For this function, Eq. (9) takes the form

$$\omega\tilde{\phi}(\omega,q) = -2\omega_G(q)\tilde{\phi}(\omega,q) + \bar{\alpha}_S\int\frac{d^2q'}{\pi}\{G^{-1}(q)G(\boldsymbol{q}-\boldsymbol{q}')G(q')\}\tilde{\phi}(\omega,q'), \tag{31}$$

The eigenfunction in the coordinate space has the form

$$\Psi(r) = \int\frac{d^2q_T}{(2\pi)^2}e^{i\boldsymbol{r}\cdot\boldsymbol{q}_T}\tilde{\phi}(q_T), \tag{32}$$

and the master equation has the form of Eq. (21) with the potential energy, which has the different form

$$\mathcal{H}\Psi(r) = \underbrace{T(\hat{\kappa})}_{\text{kineticenergy}}\Psi(r) - \int d^2r'\underbrace{U(\boldsymbol{r},\boldsymbol{r}')}_{\text{potentialenergy}}\Psi(r') \tag{33}$$

with

$$U(r,r') = \int\frac{d^2q_T}{(2\pi)^2}e^{i\boldsymbol{r}\cdot\boldsymbol{q}_T} \times\int\frac{d^2q_T'}{(2\pi)^2}e^{i\boldsymbol{r}'\cdot\boldsymbol{q}_T'}\{G^{-1}(q)G(\boldsymbol{q}-\boldsymbol{q}')G(q')\} = \int d^2r''K_0((m+m_0)|\boldsymbol{r}-\boldsymbol{r}''|) \times((-\nabla^2_{r''}+m)^2+1)G(r'')G(\boldsymbol{r}''-\boldsymbol{r}'). \tag{34}$$

One can see that for $m = m_0 = 0$ the potential energy $U(r,r') \propto ln(r)$ and Eq. (24) turns out to be incorrect. For $m \neq 0$ and $m_0 \neq 0$, the potential energy decreases exponentially at long distances. Hence, in this case, Eq. (24) holds.

C. Eigenfunctions in the vicinity of $E_0 = T(\kappa = 0)$

As we have discussed above, there is a possibility that the master equation has the eigenvalues in addition to the eigenvalues of the QCD BFKL equation. These states should have the wave functions that decrease much more steeply than the eigenfunction of Eq. (12). From Fig. 3, one can expect that the vicinity of $E = E_0 = T(\kappa = 0)$ can provide such states. Indeed, in the vicinity, $E \to E_0$ $T(\kappa)$ takes the form

$$T(\kappa) = \mathrm{Re}\left\{\frac{\tilde{m}_0\tilde{m}\tilde{m}^*}{4(m+m_0)}\left[\frac{\tilde{m}_0}{\tilde{m}}+\frac{i}{2}\tilde{m}_0{}^*\ln\left(\frac{\tilde{m}^*}{\tilde{m}}\right)\right]+\frac{\kappa\tilde{m}_0}{4}\left[\left(1-\frac{\tilde{m}_0\tilde{m}_0{}^*}{(m+m_0)^2}\right)\left(\frac{\tilde{m}_0}{\tilde{m}}+\frac{i}{2}\tilde{m}_0{}^*\ln\left(\frac{\tilde{m}^*}{\tilde{m}}\right)\right)+\frac{\tilde{m}\tilde{m}^*}{m+m_0}\left\{-\frac{\tilde{m}_0}{6\tilde{m}^2}+\tilde{m}_0{}^*\left(-\frac{1}{2}+\frac{i}{4}m\ln\left(\frac{\tilde{m}^*}{\tilde{m}}\right)\right)\right\}\right]\right\}. \tag{35}$$

$$\equiv E_0 + E_0'\kappa \tag{36}$$

Equation (10a) takes the following form in vicinity of $\kappa \to 0$:

$$(E - E_0 - E_0'\kappa)\phi(\kappa) = -\int d\kappa' K(\kappa=0,\kappa')\phi(\kappa') - \kappa\int d\kappa'\left.\frac{\partial K(\kappa,\kappa')}{\partial\kappa}\right|_{\kappa=0}\phi(\kappa') + \mathcal{O}(\kappa^2). \tag{37}$$

Introducing

$$\epsilon = \frac{E - E_0}{E_0' - \int d\kappa' \frac{\partial K(\kappa,\kappa')}{\partial \kappa}|_{\kappa=0}}$$

, one can see from Eq. (37) that $\phi(\kappa)$ has a singularity,

$$\phi(\kappa)|_{\kappa\to\epsilon} = \frac{\text{Const}}{\epsilon - \kappa}, \tag{38}$$

or, in other words, the wave function has the form

$$\phi(\kappa) = \frac{\text{Const}}{\epsilon - \kappa} + \phi_{\text{bg}}(\kappa), \tag{39}$$

where ϕ_{bg} is the function which has no singularities. Since the eigenvalue $E = E_0$ is multiple degenerate the sum of functions of Eq. (39) is also an eigenfunction.

It is instructive to note that the eigenfunctions of Eq. (39) does not appear for the QCD BFKL equation. As we have seen, the origin of such eigenfunctions is in the fact that typical κ' in Eq. (37) are about the values of mass and not equal to zero.

D. Summary

Concluding this section, we wish to emphasize two results that we have proved. First, the eigenvalues of the massless BFKL equation, generally speaking, are expected to be the eigenvalues of the master equation. In principle, it is possible that the behavior of the wave functions at small values of κ could select out some of the eigenvalues of the BFKL equation in QCD. However, because of double degeneracy of each of the massless BFKL eigenvalues [see that Eq. (14) has symmetry $\nu \to -\nu$], the boundary conditions at $\kappa \to 0$ do not lead to a loss of the eigenvalues of the master equation in comparison with the massless BFKL equation.

Second, it is possible that the eigenvalues of the master equation have a richer structure than the eigenvalues of the BFKL equation in QCD. Indeed, there could exist states with the wave functions that are suppressed at large κ: $\phi(\kappa) \ll \kappa^{-\frac{1}{2}+i\nu}$. An example of such a function could be Eq. (38). As we see from Fig. 3, the eigenfunctions with $E = E_0$ have infinite degeneracy, and all of them are eigenfunctions that have not been present in the massless BFKL equation.

The separate problem is the state with the wave function that decreases more steeply than the eigenfunction of the massless BFKL equation but with the eigenvalue which is smaller than $E_{\text{min}} = -4\ln 2$.

At the moment, we cannot answer this question without finding the numerical solution to the master equation.

IV. NUMERICAL SOLUTION

A. General approach

Generally speaking, we need to solve the equation which has the structure

$$E\phi(\kappa) = \int d\kappa' \mathcal{K}(\kappa,\kappa')\phi(\kappa'), \tag{40}$$

where $\mathcal{K}$ is defined in Eq. (10b). The advantage of using Eq. (10b) in comparison with Eq. (10a) is discussed in Appendix B of Ref. [27].

For the numerical solution, we discretize the continuous variables κ and κ' using the logarithmic grid $\{\kappa_n\}$ with $N+1$ nodes,

$$\kappa_n = \kappa_{\text{min}}\exp(n\Delta_\kappa), \quad \Delta_\kappa = \frac{1}{N}\ln(\kappa_{\text{max}}/\kappa_{\text{min}}), \quad n = 0,\ldots,N, \tag{41}$$

where the values of κ_{min} and κ_{max} are fixed. In the most details, we consider the case with $\kappa_{\text{min}} = 10^{-10}$, $\kappa_{\text{max}} = 10^{65}$ and $N = 2000$, but we investigated the dependence of the solution on the values of κ_{min}, κ_{max}, and N. In the discrete variables, Eq. (40) can be approximated in the form

$$E\phi(\kappa_n) = \sum_{m=0}^{N} \kappa_m \Delta_\kappa K(\kappa_n,\kappa_m)\phi(\kappa_m). \tag{42}$$

Introducing the notations $\phi(\kappa_n) \equiv \phi_n$ and $\kappa_m\Delta_\kappa\mathcal{K}(\kappa_n,\kappa_m) \equiv \mathcal{K}_{nm}$, we can rewrite Eq. (42) in the matrix form

$$E\phi_n = \sum_{m=0}^{N} \mathcal{K}_{nm}\phi_m \quad \text{or} \quad E\phi = \mathbf{K}\phi, \tag{43}$$

where vector ϕ has $N+1$ components ϕ_n and $\mathbf{K}$ is the $(N+1)\times(N+1)$ matrix. We need to find the roots of the characteristic polynomial $p(E)$ of the matrix $\mathbf{K} - E\mathbf{I}$ where $\mathbf{I}$ is the identity matrix. Hence, we need to solve the secular equation

$$p(E) = \det(\mathbf{K} - E\mathbf{I}) = 0. \tag{44}$$

We solve Eq. (44) for several equations. First, we found the solution to our new Eq. (10b) in two cases: for the Gribov propagator of Eq. (2) and for the propagator of Eq. (11e). In the first case, we need to put $m = 0$ and $m_0 = 0$ in Eqs. (11a)–(11e), while in the second, we need to choose $m = 1.27$ and $m_0 = 3.76$ in these equations. It should be recalled that we use the dimensionless variables of Eq. (6) and the scale for dimensionful observables is $\mu^2 = 0.48$ GeV^2 [44]. Second, we solve the original BFKL equation for QCD, which has the form

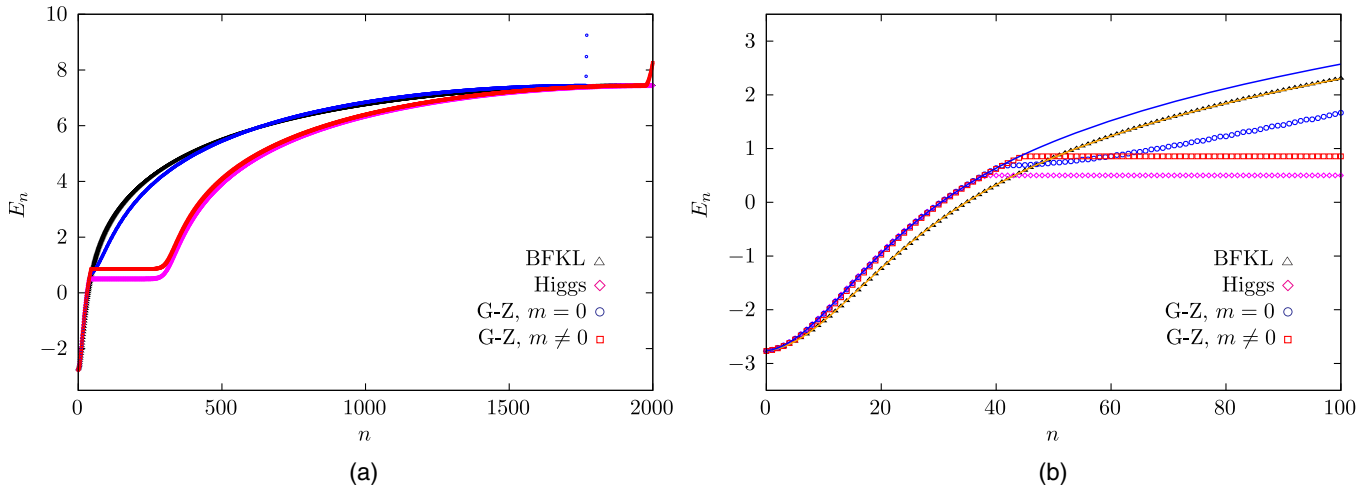

FIG. 5. The eigenvalues E_n of four equations: the BFKL equation in QCD [BFKL; see Eq. (45)], the BFKL equation for the modle [Higgs; see Eq. (46)], for Eq. (10b) in the case of the Gribov propagator (G-Z, $m = 0$), and in the case of thelattice QCD propagator of Eq. (3) (G-Z, $m \neq 0$). The solid lines in Fig. 5(b) show the eigenvalues calculated using Eq. (47) with β_n, that were taken from the pattern of zeros of the eigenfunctions given by Eqs. (49), (50), and (52). All results correspond to solutions with $\kappa_{\min} = 10^{-10}$, $\kappa_{\max} = 10^{65}$, and grid size $N = 2000$ [see Eq. (41)].

$$E\phi_{\rm BFKL}(\kappa) = -\int \frac{d\kappa'}{|\kappa-\kappa'|}\left(\phi_{\rm BFKL}(\kappa') - \frac{\kappa}{\kappa'}\phi_{\rm BFKL}(\kappa)\right) - \int \frac{\kappa d\kappa'}{\kappa'\sqrt{\kappa^2+4\kappa'^2}}\phi_{\rm BFKL}(\kappa). \tag{45}$$

We believe that we need to compare our numerical procedure with the equation which has the analytical solution, both to check the accuracy of our numerical estimates and to evaluate our transition to the continuous limit. Recall that the numerical solution gives the discrete spectrum of the eigenvalues instead of the continuous one.

In addition, we solve the equation, which was derived in Ref. [22] for non-Abelian gauge theory with the Higgs mechanism for mass generation. This theory is not QCD, since it has no confinement of quarks and gluons. However, it has the same color structure as QCD and introduces the dimensional scale: the mass of Higgs boson. Solving the BFKL equation for this theory, we could find out what is more essential: the new dimensional scale or specifics related to the confinement. Below, we will call this approach "the model," and the main BFKL equation for this model takes the form

$$E\phi(\kappa) = \underbrace{\frac{\kappa+1}{\sqrt{\kappa}\sqrt{\kappa+4}}\ln\frac{\sqrt{\kappa+4}+\sqrt{\kappa}}{\sqrt{\kappa+4}-\sqrt{\kappa}}\phi(\kappa)}_{\text{kinetic energy term}} - \underbrace{\int_0^\infty \frac{d\kappa'\phi(\kappa')}{\sqrt{(\kappa-\kappa')^2+2(\kappa+\kappa')+1}}}_{\text{potential energy term}} + \underbrace{\frac{N_c^2+1}{2N_c^2}\frac{1}{\kappa+1}\int_0^\infty \frac{\phi(\kappa')d\kappa'}{\kappa'+1}}_{\text{contact term}}. \tag{46}$$

This equation has been investigated in detail. In Ref. [22], it is proven that the solution of this equation coincides with the solution to the massless BFKL equation, which is known analytically and can be used as a control of the accuracy of our numerical calculations.

B. Eigenvalues: The general characteristics

The eigenvalues of these four equations are shown in Fig. 5. One can see that (1) numerical estimates do not show the discrete eigenvalues with energy $E < E_{\min} = -4\ln 2$, where $E_{\min}$ is the minimal energy of the massless BFKL equation, and (2) none of the eigenvalues of the massless BFKL equation has been selected out in accord with our expectations in Sec. III A.

From Fig. 5, we see that all eigenvalues can be divided in three regions: the eigenvalues $E_n \leq E_0 = T(\kappa = 0)$, the multiply degenerate eigenvalue E_0, and $E_n \geq E_0$.

For $E_{\min} \leq E_n \leq E_0$, there are no other eigenvalues except the massless BFKL ones. Indeed, we can describe these eigenvalues using the following formulas:

$$E(n) = -2\psi(1) + \psi\left(\frac{1}{2}+i\beta(n)\right) - \psi\left(\frac{1}{2}-i\beta(n)\right)$$
$$\beta(n) = a_\beta(n+1), a_\beta = c_\beta/\ln(\kappa_{\max}/m_\beta^2). \tag{47}$$

For the QCD BFKL equation, $c_\beta = 3.015$ and $m_\beta^2 = \kappa_{\min}$, while for all other three equations, we can put $c_\beta = 3.140$ and $m_\beta^2 = 0.0042$ [see Fig. 9(a)]. Hence,

TABLE I. The first 20 eigenvalues E_n for the BFKL equation in QCD [QCD; see Eq. (45)]; for the model, developed in Ref. [22] [Higgs; see Eq. (46)]; for Eq. (10b) in the case of the Gribov propagator (G-Z $m = 0$); and in the case of lattice QCD propagator of Eq. (3) (G-Z, $m \neq 0$). The last column contains values defined by Eq. (47).

n	E_n (QCD)	E_n (Higgs)	E_n (G-Z, $m = 0$)	E_n (G-Z, $m \neq 0$)	E_n [Eq. (47)]
0	−2.7675	−2.7657	−2.7660	−2.7666	−2.7657
1	−2.7519	−2.7448	−2.7457	−2.7483	−2.7452
2	−2.7261	−2.7103	−2.7123	−2.7178	−2.7114
3	−2.6905	−2.6630	−2.6665	−2.6753	−2.6650
4	−2.6456	−2.6036	−2.6088	−2.6211	−2.6067
5	−2.5919	−2.5332	−2.5403	−2.5561	−2.5377
6	−2.5301	−2.4529	−2.4620	−2.4810	−2.4588
7	−2.4610	−2.3640	−2.3751	−2.3968	−2.3715
8	−2.3854	−2.2677	−2.2808	−2.3048	−2.2768
9	−2.3040	−2.1653	−2.1802	−2.2060	−2.1760
10	−2.2177	−2.0581	−2.0746	−2.1018	−2.0705
11	−2.1273	−1.9472	−1.9651	−1.9932	−1.9612
12	−2.0336	−1.8337	−1.8528	−1.8815	−1.8492
13	−1.9373	−1.7186	−1.7387	−1.7675	−1.7356
14	−1.8391	−1.6029	−1.6236	−1.6523	−1.6212
15	−1.7397	−1.4872	−1.5083	−1.5368	−1.5068
16	−1.6396	−1.3724	−1.3936	−1.4215	−1.3930
17	−1.5394	−1.2588	−1.2800	−1.3072	−1.2804
18	−1.4395	−1.1470	−1.1680	−1.1944	−1.1695
19	−1.3403	−1.0374	−1.0579	−1.0835	−1.0605
20	−1.2421	−0.9303	−0.9501	−0.9748	−0.9539

Fig. 5(b) and Table I demonstrate a new phenomenon: the eigenvalues of all three equations, which introduce a dimensional scale in the BFKL approach, turn out to be the same. Actually, they are the eigenvalues of the QCD BFKL equation, as shown in Eq. (47) and Fig. 5(b). In Fig. 5, the eigenvalues from Eq. (47) are shown by the solid lines, and one can see that all these values for $E_n \leq E_0$ can be perfectly described by this equation. Equation (47) can be interpreted as an indication that the transition to the continuous limit reduces to replacement $\frac{1}{2} + i\beta(n) \to \frac{1}{2} + i\nu \equiv \gamma$. In these new variables, the eigenvalues of the QCD BFKL looks familiar [2]:

$$E(\gamma) = -2\psi(1) + \psi(\gamma) - \psi(1-\gamma). \tag{48}$$

Table I, in which we put the first 20 roots of the secular equation, illustrates these points. First, we see that the solution to the QCD BFKL equation gives the eigenvalues, which are quite close to the analytical estimates [see Eq. (47)]. This indicates that our method of numerical

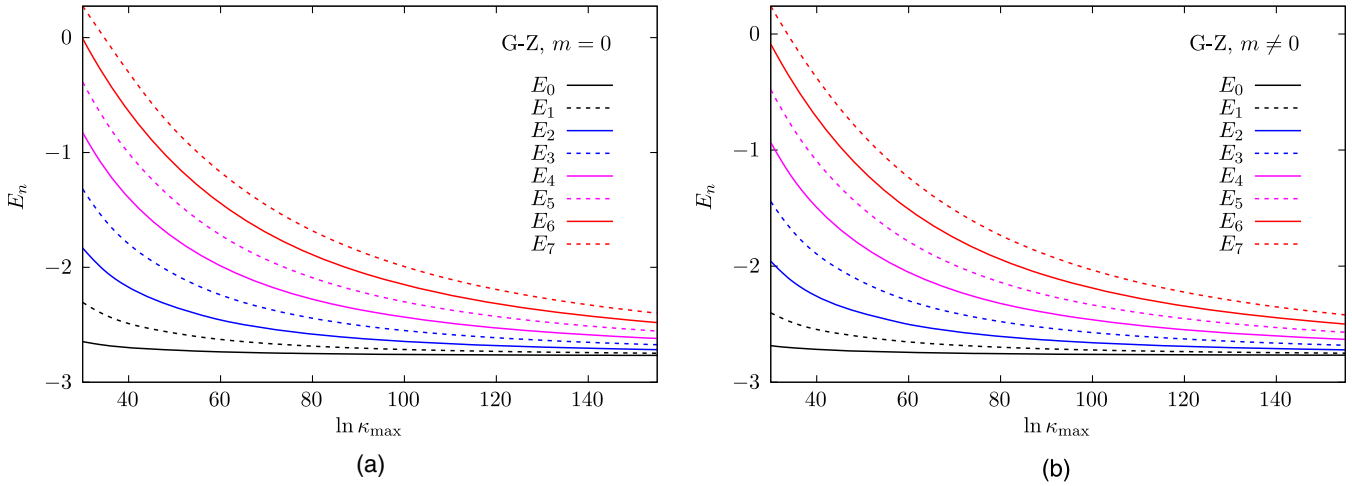

FIG. 6. The first several eigenvalues of Eq. (10a) vs $\ln(\kappa_{\max})$. Figure 6(a) for the Gribov propagator of Eq. (2) and Fig. 6(b) for the lattice propagator of Eq. (3).

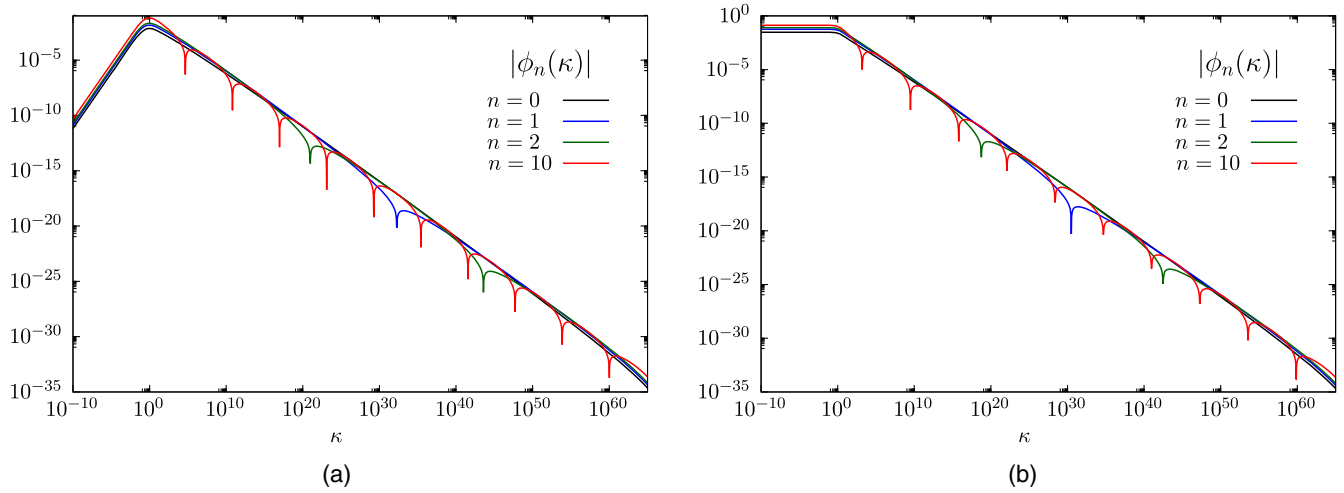

FIG. 7. The examples of the eigenfunctions of Eq. (10b). Figure 7(a) for the Gribov propagator of Eq. (2), i.e., $m = 0, m_0 = 0$ in Eq. (11e). Figure 7(b) for the lattice QCD propagator of Eq. (11e) with $m = 1.27, m_0 = 3.76$. Functions $\phi_n(\kappa)$ for $n = 0$, 1, 2 and 10. One can see that every $\phi_n(\kappa)$ has n zeros.

solving provides a good accuracy. As we can see, in both cases, the lowest eigenvalue becomes quite close to $E_{\min} = -4\ln 2$ and the difference is negligibly small (of the order of 5×10^{-3} for $\kappa_{\min} = 10^{-10}$ and $\kappa_{\max} = 10^{65}$). Figure 6 shows the dependence of the first seven roots versus the value of $\kappa_{\max}$. One can see that when $\kappa_{\max}$ grows ($\kappa_{\max} \to \infty$) the distance between neighboring roots decreases rapidly, inferring the smooth transition to the continuous limit.

As we can see from Fig. 5 at $E_n = E_0 = T(\kappa = 0)$ for three equations, that introduce a new dimensional scale, we have multiple degenerate eigenvalues. For the Gribov propagator, this degeneration is not very large, but in other cases, it is so large that we can expect something like Bose-Einstein condensation at this energy. We have discussed the general structure of the eigenfunction at this value of energy in Sec. III C and will consider it below. For the scattering amplitude, all these eigenfunctions correspond to the cross sections that decrease as a power of energy and, because of this, do not show up in the high energy scattering processes.

C. Eigenfunctions for $E \le E_0 = T(\kappa = 0)$

For the QCD BFKL equation [see Eq. (45)], the eigenfunctions are given by Eq. (12), and for the numerical solutions, they take the form

$$\phi_n^{\mathrm{BFKL}}(\kappa) = \frac{\alpha_n}{\sqrt{\kappa}} \sin(\beta_n \ln\kappa + \varphi_n). \tag{49}$$

The eigenfunctions for Eq. (46) are discussed in Ref. [22] and can be described as follows:

$$\phi_n(\kappa) = \frac{1}{\sqrt{\kappa+4}} \sin(\beta_n \mathrm{Ln}(\kappa) + \varphi_n), \tag{50}$$

where

$$\mathrm{Ln}(\kappa) = \frac{\sqrt{\kappa+4}+\sqrt{\kappa}}{\sqrt{\kappa+4}-\sqrt{\kappa}} \xrightarrow{\kappa\gg 1} \ln(\kappa) \tag{51}$$

Several examples of the eigenfunctions for Eq. (10b) are shown in Fig. 7. One can see that the number of zeros follows the usual pattern of a quantum mechanical approach: the minimum energy state has no zeros. The next has one, and so on. At large κ, $\phi_n(\kappa) \propto \sin(\alpha_\beta n \ln\kappa)$, or in other words, $\phi_n(\kappa) = C_1 \phi_{\mathrm{BFKL}}(\kappa; \frac{1}{2} + i\beta_n) + C_2 \phi_{\mathrm{BFKL}}(\kappa; \frac{1}{2} - i\beta_n)$, where $\phi_{\mathrm{BFKL}}(\kappa;\gamma)$ are given by Eq. (12).

For $\kappa \ge 1$, all eigenfunctions can be parametrized in the following way:

$$\phi_n(\kappa) = \frac{\alpha_n(\kappa+m)}{\sqrt{(\kappa+a_n)^3}} \sin(\beta_n Ln(\kappa) + \varphi_n), \tag{52}$$

where

$$Ln(\kappa) = \frac{\kappa}{4}\{\mathrm{Re}(\tilde{m}_0{}^2 I_1) + \tilde{m}_0 \tilde{m}_0{}^* I_2\} \xrightarrow{\kappa\gg 1} \ln\kappa. \tag{53}$$

Parameter β_n has the simple form defined by Eq. (47):

$$\beta_n = a_\beta(n+1), \qquad a_\beta = \frac{3.140}{\ln(\kappa_{\max}/m_\beta^2)}. \tag{54}$$

It was found that for the Gribov propagator ($m = 0$, $m_0 = 0$) and for the propagator with $m \neq 0$, $m_0 \neq 0$ the same $m_\beta^2 = 0.0042$ can be used [see Fig. 9(a)]. While φ_n needs a bit more complicated parametrization:

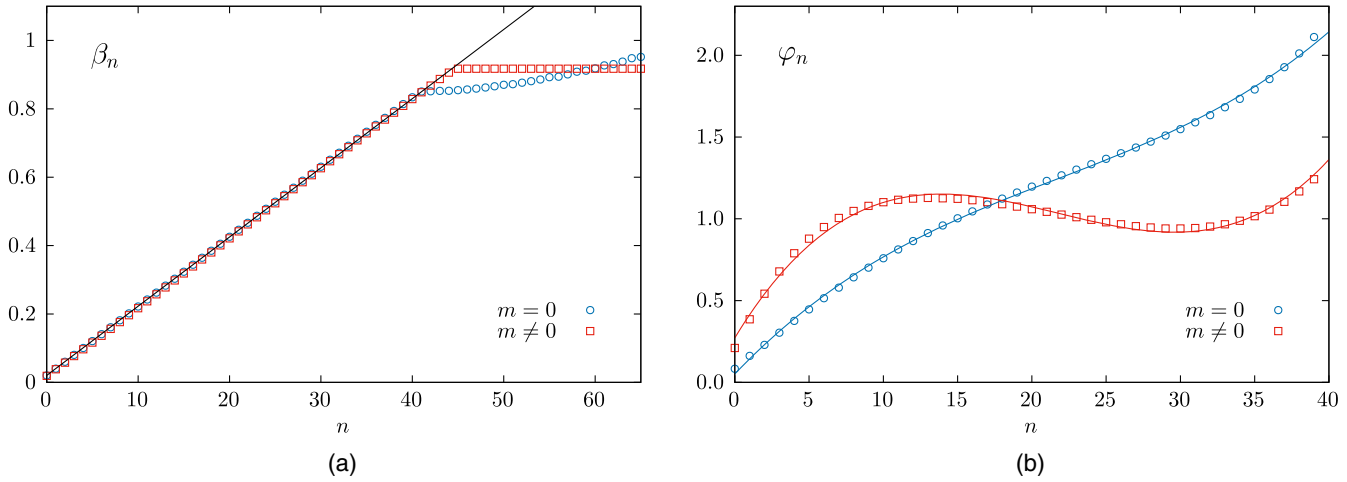

FIG. 8. Parameters β_n [Fig. 8(a)] and φ_n [Fig. 8(b)] of Eq. (52) for the eigenfunctions $\phi_n(\kappa)$ vs n. Presented data correspond to the eigenfunctions obtained with $\kappa_{\min} = 10^{-10}$ and $\kappa_{\max} = 10^{65}$. One can see that β_n has simple linear dependence while φ_n has a more complicated form given by Eq. (55). Solid lines correspond to the proper parametrizations [i.e., Eq. (54) for β_n and Eq. (55) for φ_n].

$$\varphi_n = a_{\varphi,0} + a_{\varphi,1} n + a_{\varphi,2}(n - n_\varphi)^3. \tag{55}$$

For $\kappa_{\max} = 10^{65}$, we obtain the following values for parameters $a_{\varphi,i}$:

$$a_{\varphi,0} = 0.486(1.520); \qquad a_{\varphi,1} = 0.0350(-0.0223);$$
$$a_{\varphi,2} = 0.425 \times 10^{-4}(1.211 \times 10^{-4}); \quad n_\varphi = 21.71(21.76). \tag{56}$$

In Eq. (56), the values of $a_{\varphi,i}$ for the case $m \neq 0, m_0 \neq 0$ are given in parentheses. Figure 8 shows the n dependence of β_n and ϕ_n for $n \leq 40$. One can see that the linear dependence of Eq. (54) holds for β_n, but φ_n shows a more complicated pattern: $\varphi_n \propto n$ with variations described by Eq. (55). Figure 9(a) shows the dependence of a_β on the value of $\kappa_{\max}$ for Gribov's ($m = 0$) and lattice QCD ($m \neq 0$) gluon propagators. One can see that Eq. (54) describes this dependence quite well.

As far as dependence on $\kappa_{\max}$ of β_n, φ_n, and a_n is concerned, we found that they have quite a simple scaling property, which allows us to relate their values obtained with different $\kappa_{\max}$: values of some parameter $P_n = P(n;\kappa_{\max 1})$ corresponding to $\kappa_{\max 1}$ fit well to results $P(n;\kappa_{\max 2})$ after simple change of the scale of n,

$$P(n;\kappa_{\max 1}) \approx P(nS;\kappa_{\max 2}), \qquad S = \frac{\ln(\kappa_{\max 2})}{\ln(\kappa_{\max 1})} \tag{57}$$

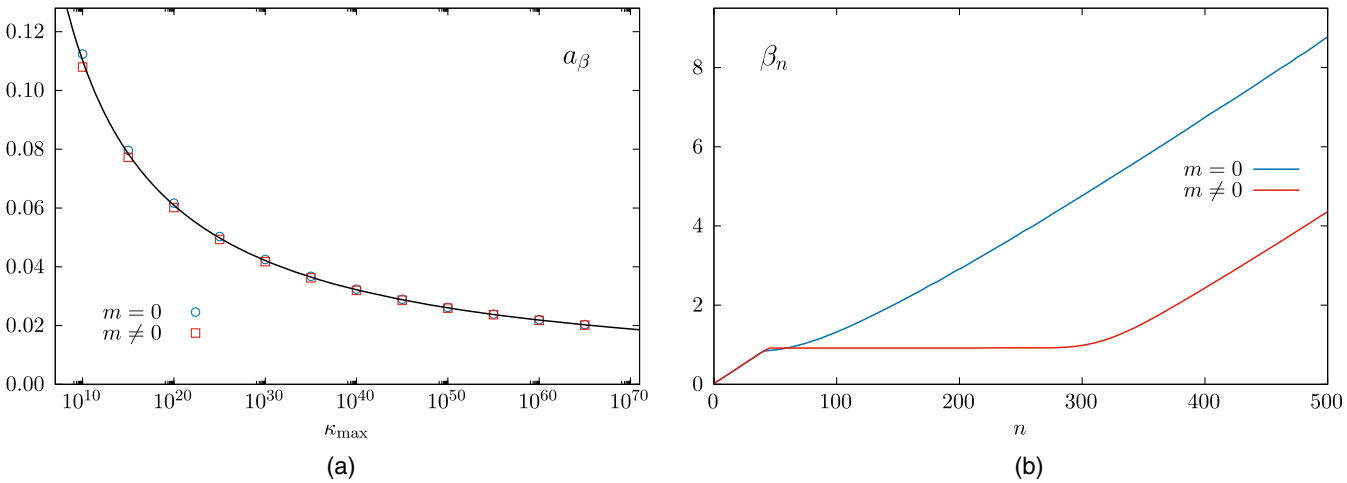

FIG. 9. Figure 9(a): a_β vs $\kappa_{\max}$ for Gribov's and lattice QCD gluon propagators. The solid line corresponds to Eq. (54) with $m_\beta^2 = 0.0042$ for both cases. Figure 9(b): β_n of Eq. (52) for the eigenfunctions $\phi_n(\kappa)$ obtained with $\kappa_{\min} = 10^{-10}$ and $\kappa_{\max} = 10^{65}$ at $\kappa > 1$ vs n.

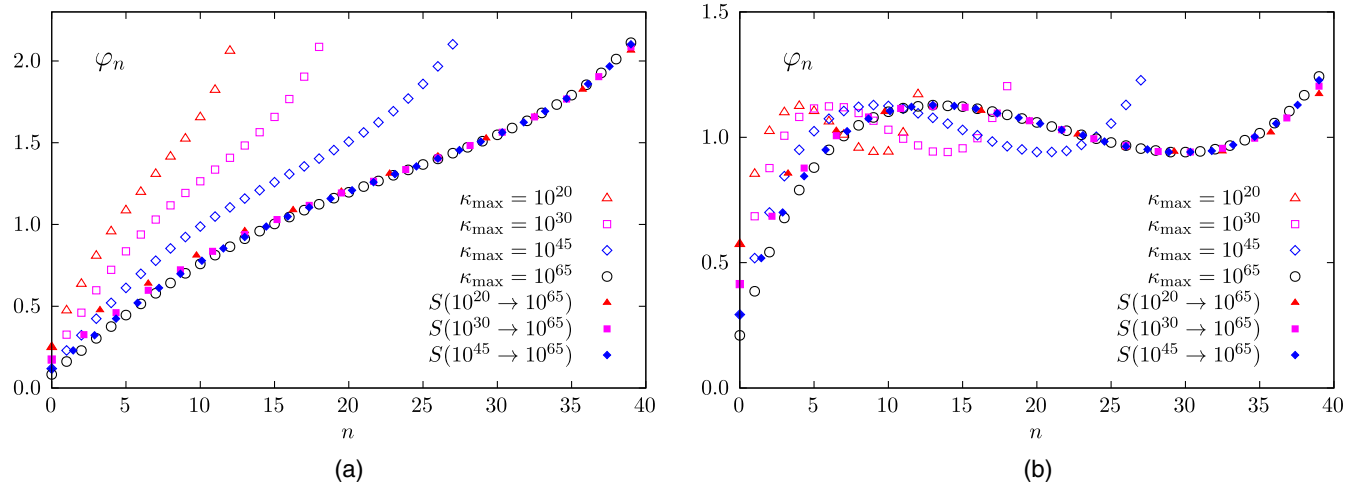

FIG. 10. Scaling on $\kappa_{\max}$ for parameter φ_n. Values on Fig. 10(a) correspond to the Gribov's gluon propagator and on Fig. 10(b) to the lattice QCD propagator. Open symbols denote parameter obtained at different $\kappa_{\max} = 10^{20}, 10^{30}, 10^{45}, 10^{65}$. Sets of φ scaled on n to $\kappa_{\max} = 10^{65}$ are denoted by appropriate solid symbols.

Such scaling behavior for β_n follows from Eq. (54), while Fig. 10 illustrates such $\kappa_{\max}$ scaling for parameter φ_n. The figure shows parameters obtained at different $\kappa_{\max}$ in the range from 10^{20} to 10^{65}. Sets of φ were scaled on n with the proper coefficient [see Eq. (57)] to $\kappa_{\max} = 10^{65}$. One can see that "scaled" points are in good agreement with original values for $\kappa_{\max} = 10^{65}$.

For the Gribov propagator, the eigenfunction $\phi_n(\kappa) \propto \kappa$ in the region of small κ. In other words, the eigenfunctions in the coordinate space exhibit the powerlike decrease at long distances. It turns out that for small κ we can use Eq. (52), which introduces the dependence of parameter a_n on n. Figure 11(a) shows the scaling behavior of Eq. (57) for a_n in the case of Gribov's propagator. It should be stressed that the same scaling behavior holds for the case of $m \neq 0$.

Figure 11(b) shows the dependence of a_n on n. From this figure, we see that $a_n \propto n^2$ for the Gribov's propagator with $a_n = 0.3$ at $n = 0$. In other words, the typical κ turns out to be in the region of $\kappa = 0.27 \div 0.75$. It should be stressed that Eq. (52) describes quite well the behavior of the eigenfunctions both at large $\kappa \geq 1$ and at small $\kappa \leq a_n$, but at $\kappa \sim a_n$, Eq. (52) does not lead to a good fit of the eigenfunctions. For the case of the lattice QCD propagator [Eq. (11e) with $m = 1.27$ and $m_0 = 3.76$], Fig. 11(b) shows that a_n decreases with n approaching $a_n \approx 0.4$ at $n \to 40$. One can see that for small n the typical values of $\kappa \sim 1$. and the range of typical κ is $0.4 \div 1$. We would like to

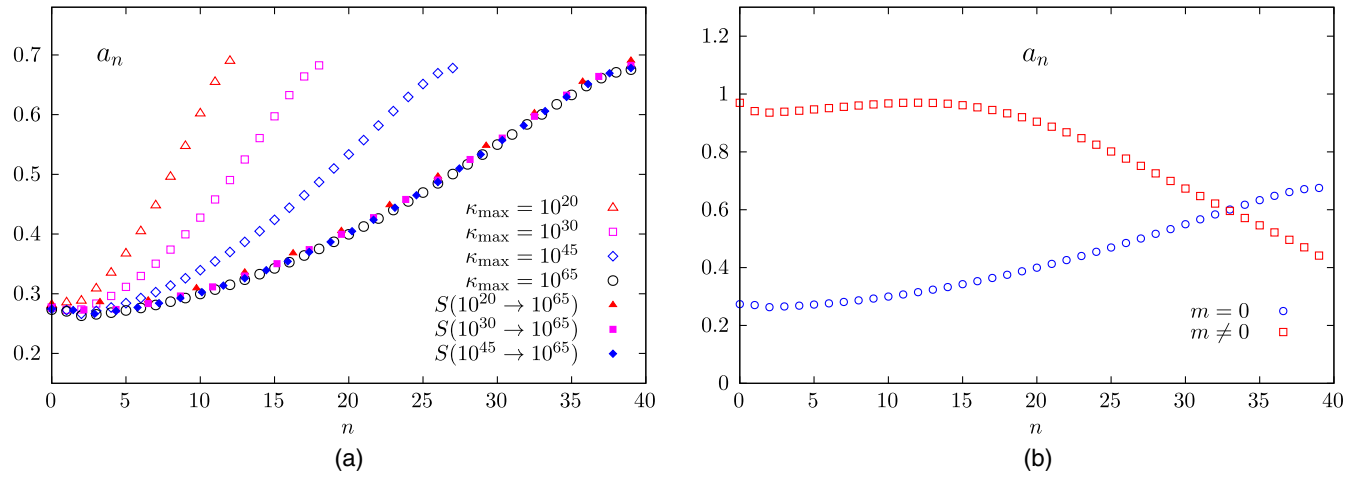

FIG. 11. Values of parameter a_n from the Eq. (52) vs n. Figure 11(a) demonstrates scaling property of this parameter for the case with Gribos's propagator. Figure 11(b) shows a_n for both variants (i.e., Gribov's and QCD propagators) corresponding to eigenfunctions with $\kappa_{\min} = 10^{-10}$ and $\kappa_{\max} = 10^{65}$.

stress that the value of a_n cannot be viewed as a typical scale for the κ dependence of the eigenfunctions. Indeed, one can see directly from Fig. 7 that the typical κ is about $\kappa \sim 1$ for both cases.

D. Eigenfunctions for $E_n = E_0 = T(\kappa = 0)$

As we have discussed above, the solution leads to the multiple degenerate state at $E_n = E_0 = T(\kappa = 0)$. Using Eq. (47), we can estimate the value of β^0, viz., $E_0 = -2\psi(1) + \psi(\frac{1}{2} + i\beta^0) + \psi(\frac{1}{2} - i\beta^0)$. The corresponding eigenfunction index n, where the first degenerate eigenvalue appears, can be estimated using Eq. (54): the degenerate eigenfunction sequence starts when β_n reaches value β^0. For the Gribov propagator, $\beta^0 \approx 0.85$ [see Fig. 8(a)] leads to the value $n = 41$ in the case with $\kappa_{\max} = 10^{65}$, while for the RGZ gluon propagator, $\beta^0 \approx 0.92$ gives $n = 45$ [see Fig. 8(a)]. At such values of n, the κ behavior of the eigenfunctions shows a discontinuity in κ: of course, numerical values of eigenfunctions at $\ln(\kappa/\kappa_{\min}) = n\Delta$ [see Eq. (41)] are still finite, but the values in the neighboring nodes have a different sign and derivative, indicating that eigenfunctions have pole in κ located somewhere between nodes.

The structure of the eigenfunctions with this eigenvalue is rather simple for the lattice (RGZ) QCD gluon propagator [see Eq. (11e) with $m = 1.27$ and $m_0 = 3.76$], and it is close to 1, which is discussed in Ref. [22] for Eq. (46). The eigenfunctions for $E_n = E_0$ have poles in $\kappa = \kappa_{p,n}$ as has been shown in Sec. III C. Actually, the minimal value of $\kappa_{p,n}$ is equal to $\kappa_{\min}$ [strictly speaking, the first pole is located somewhere between the first node $\kappa_0 = \kappa_{\min}$ and the next node $\kappa_1 = \kappa_{\min}\exp(\Delta_\kappa) \approx \kappa_{\min}(1 + \Delta_\kappa)$]. With each increase of the n, the pole moves exactly to the next interval on κ (i.e., the second pole is located between κ_1 and κ_2 and so on). This sequence terminates when the pole reaches the maximal value of $\kappa = \kappa^0 \approx 3$, where κ^0 is the location of the first zero of the eigenfunction of Eq. (52). All eigenfunctions with $E_n = E_0$ have the same number of zeros. All these features can be seen from Fig. 12.

Generally, for $m \neq 0$ and $m_0 \neq 0$, the eigenfunction can be approximated by the following expression:

$$\phi_n^{(\text{approx})}(\kappa) = \frac{a_{p,n}}{\kappa_{p,n} - \kappa} + \phi_n(\kappa; \text{Eq. (52)}) = \frac{a_{p,n}}{\kappa_{p,n} - \kappa} + \frac{\alpha_n(\kappa + m)}{\sqrt{(\kappa + a_n)^3}} \sin(\beta^0 Ln(\kappa) + \varphi_n). \tag{58}$$

Eq. (58), having β^0 [see Fig. 9(b)], which does not depend on n, reflects the fact that for all these states the behavior of the eigenfunctions at large $\kappa \geq 1$ can be described by one function with the same number of zeros. Figure 13 shows the n dependence of other parameters of $\phi_n^{(\text{approx})}(\kappa)$ [see Eq. (58)]. One can see that the position of the pole $\kappa_{p,n}$ and its residue $a_{p,n}$ are proportional to n ($\ln(\kappa_{p,n}) \propto n, \ln(a_{p,n}) \propto n$), while the parameters of $\phi_n(\kappa; \text{Eq. (52)})$: a_n and φ_n do not depend on n in the range $n = 50$–250 which corresponds to $E_n = E_0$. The value of $a_n = 1$ gives us the typical transverse momentum $q = \mu$ [see Eq. (6)].

For Gribov's gluon propagator, the structure of the eigenfunction with $E_n = E_0$ is much more complex. First, one can notice from Fig. 14 that the number of zeros

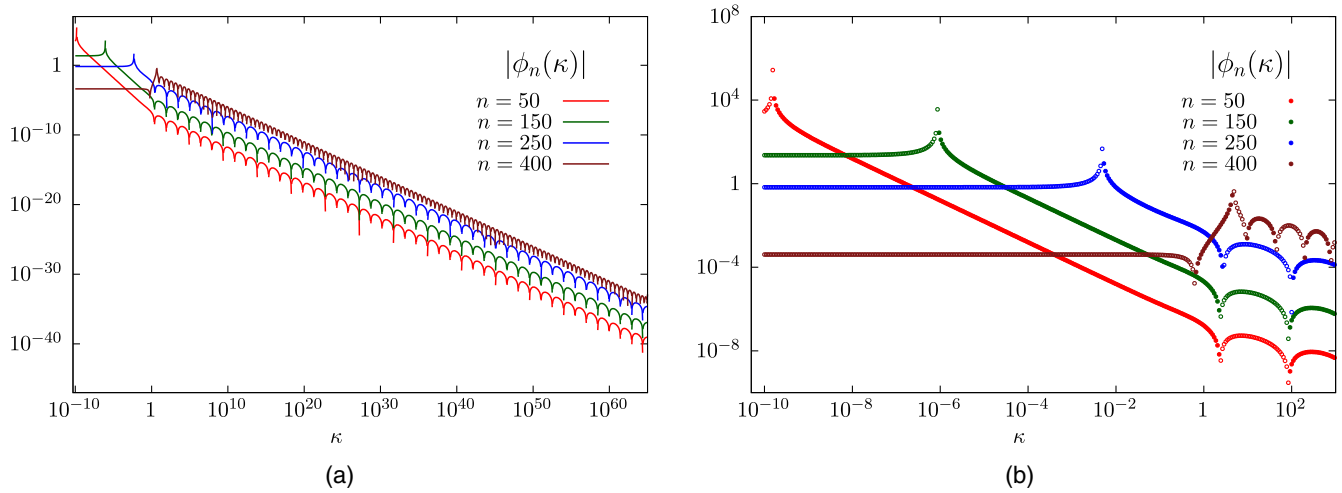

FIG. 12. The examples of the eigenfunctions with the eigenvalue $E_n = E_0 = T(\kappa = 0)$ for the lattice QCD gluon propagator [Eq. (11e) with $m = 1.27$ and $m_0 = 3.76$]. Figure 12(a) shows $\phi_n(\kappa)$ vs κ with $n = 50$, 150, 250 for which $E_n = E_0$ and $\phi_{400}(\kappa)$ with $E_{400} > E_0$. One can see that all eigenfunctions with $E_n = E_0$ have the same number of zeros. The same eigenfunctions are shown in Fig. 12(b) but in the region of small $\kappa \leq 100$. It is clearly seen that $\phi_n(\kappa)$ have the pole whose position moves from $\kappa_{\min}$ to $\kappa \approx 1$. Function $\phi_{400}(\kappa)$ has a different number of zeroes, which corresponds to increase of the value of β in Eq. (58).

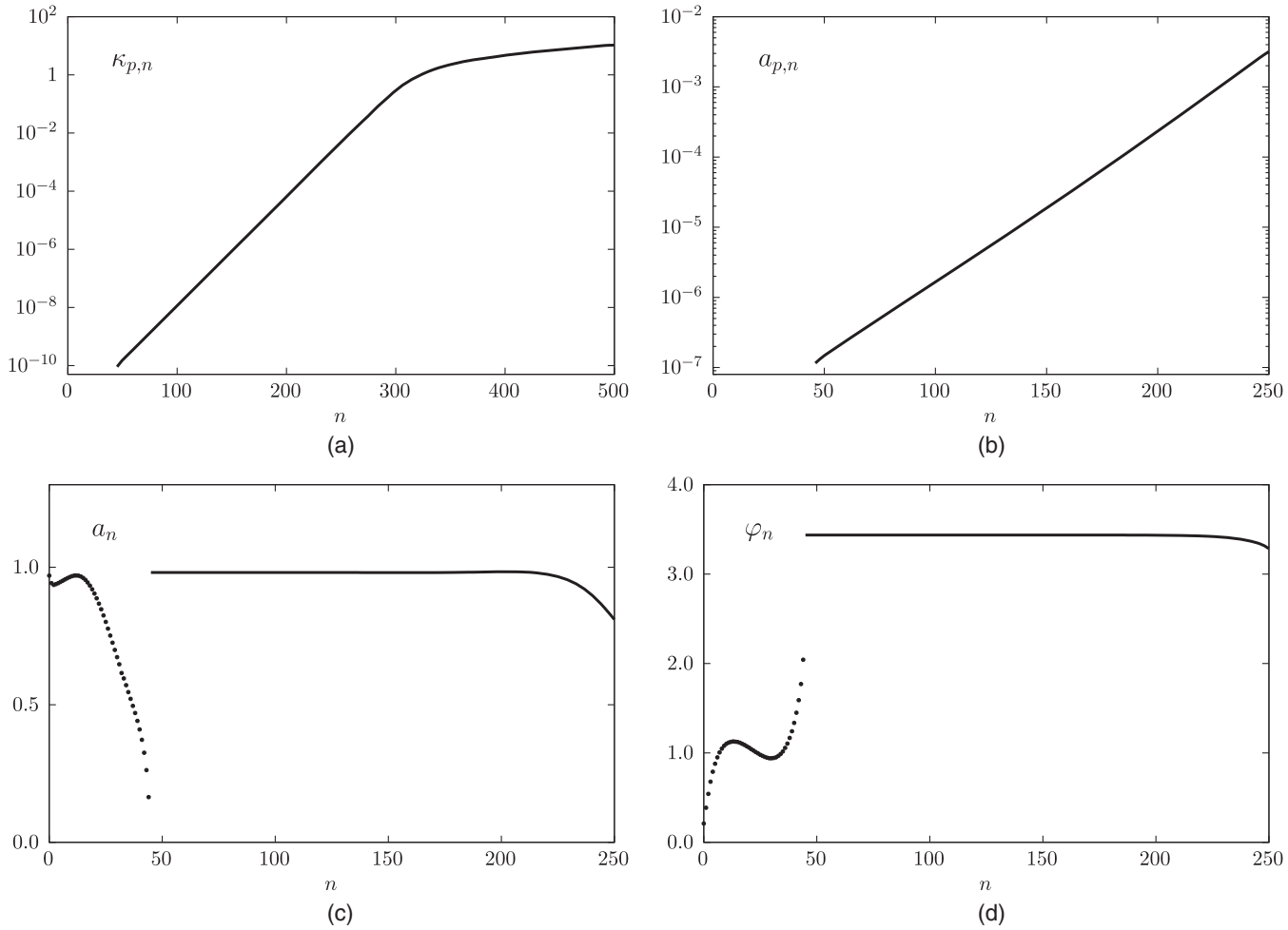

FIG. 13. Parameters of the wave functions with $E_n = E_0$ vs n. Figure 13(a) shows the position of the pole $k_{p,n}$ in Eq. (52) as a function of n, while Fig. 13(b) presents the n dependence of the residue $a_{p,n}$. Figure 13(c) and Fig. 13(d) describe the dependence of parameters a_n and φ_n on n.

is not the same for these eigenfunction but β^0 in Eq. (59) changes with n rather slowly [see Fig. 8(a) for n in the region $n = 41 \div 70$].

Second, we see that $\phi_n(\kappa)$ with $E_n = E_0$ have two poles. The first pair of poles $\kappa_{p,1} < \kappa_{p,2}$ appears near $\kappa \approx 1$. With the increase of n, the smaller one ($\kappa_{p,1}$) decreases, while $\kappa_{p,2}$ increases. On each increment of n, only one of $\kappa_{p,i}$ moves to the neighboring κ interval between nodes. So, the distance between these poles (in terms of the index of κ nodes) each time increases exactly on 1. The contribution of each of these poles vanishes at $\kappa \to 0$, and residues of these poles can have the same or opposite sign.

Third, the positions of the poles are in the region $\kappa = 0.1 \div 10$, and they exist also in the eigenfunctions with $E_n > E_0$. Fourth, two poles in the eigenfunctions have close positions. Equation (59) reflects the main features that we have discussed, but the actual structure of the eigenfunction turns out to be much more complex. However, for the Gribov propagator ($m = 0, m_0 = 0$), the eigenfunction vanishes at $\kappa = 0$ and can be approximated as follows:

$$\phi_n^{(\text{approx})}(\kappa) = \frac{\kappa a_{p,1}(n)}{\kappa^2 - \kappa_{p,1}^2(n)} \pm \frac{\kappa a_{p,2}(n)}{\kappa^2 - \kappa_{p,2}^2(n)} + \frac{\alpha_n \kappa}{\sqrt{(\kappa + a_n)^3}} \sin(\beta^0 L n \kappa + \varphi_n). \quad (59)$$

The appearance of two poles in Eq. (59) looks natural (see Sec. III C) due to multiple degeneracy of this eigenvalue. Indeed, due to this, the sum of two functions with one pole in each is also the eigenfunction. Figure 15 demonstrates that the region of n for the degenerate states with $E_n = E_0$ is very narrow but the structure of the eigenfunction with two poles lasts for $E_n > E_0$.

E. Eigenfunctions for $E_n > E_0 = T(\kappa = 0)$

For $E_n > E_0$, the eigenfunctions take the form for $\kappa > 1$

$$\phi_n(\kappa) = \frac{\alpha_n}{\sqrt{\kappa}} \sin(\beta_n L n(\kappa) + \varphi_n) \quad (60)$$

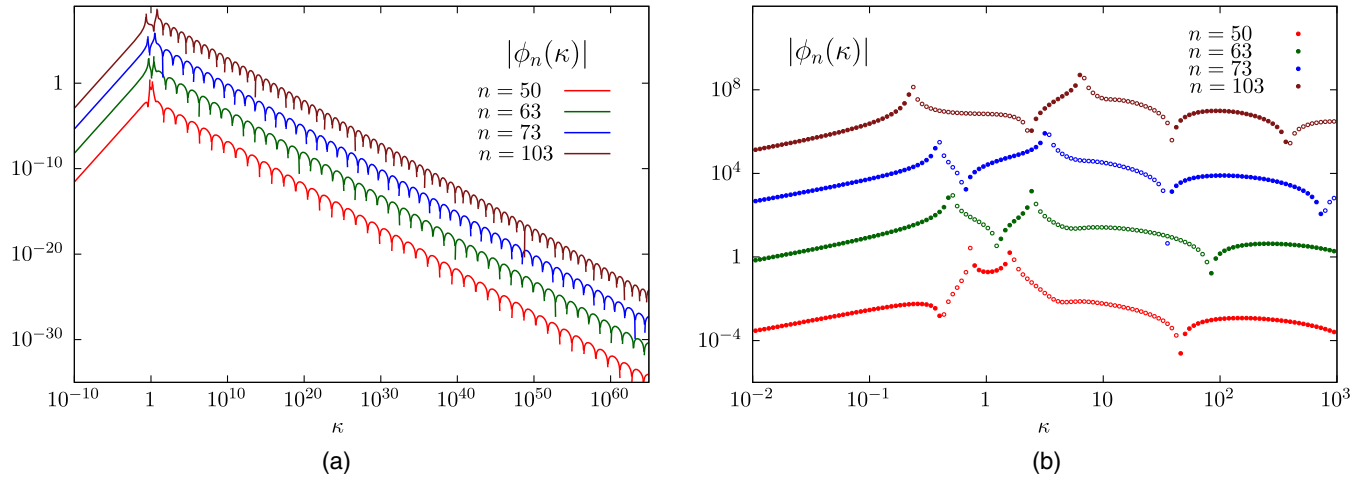

FIG. 14. The examples of the eigenfunctions with the eigenvalue $E_n = E_0 = T(\kappa = 0)$ for Gribov's gluon propagator [Eq. (11e) with $m = 0$ and $m_0 = 0$]. Figure 14(a) shows $\phi_n(\kappa)$ vs κ with $n = 50$, 63, 73 for which $E_n \approx E_0$ and $\phi_{103}(\kappa)$ with $E_{103} > E_0$. (For better clarity, some functions were scaled: values for $n = 63$ are multiplied by 10^3, $n = 73$ are multiplied by 10^6, and $n = 103$ are multiplied by 10^9.) One can see that all eigenfunctions with $E_n = E_0$ have approximately the same number of zeros, but β in Eq. (59) is not a constant but slowly grows as n increase. In Fig. 14(b), the same functions are shown in the region of small $\kappa \leq 100$. It is clearly seen that $\phi_n(\kappa)$ have two poles whose positions move in opposite directions from $\kappa = 1$. The open circles in Fig. 14(b) show the region where the function is negative.

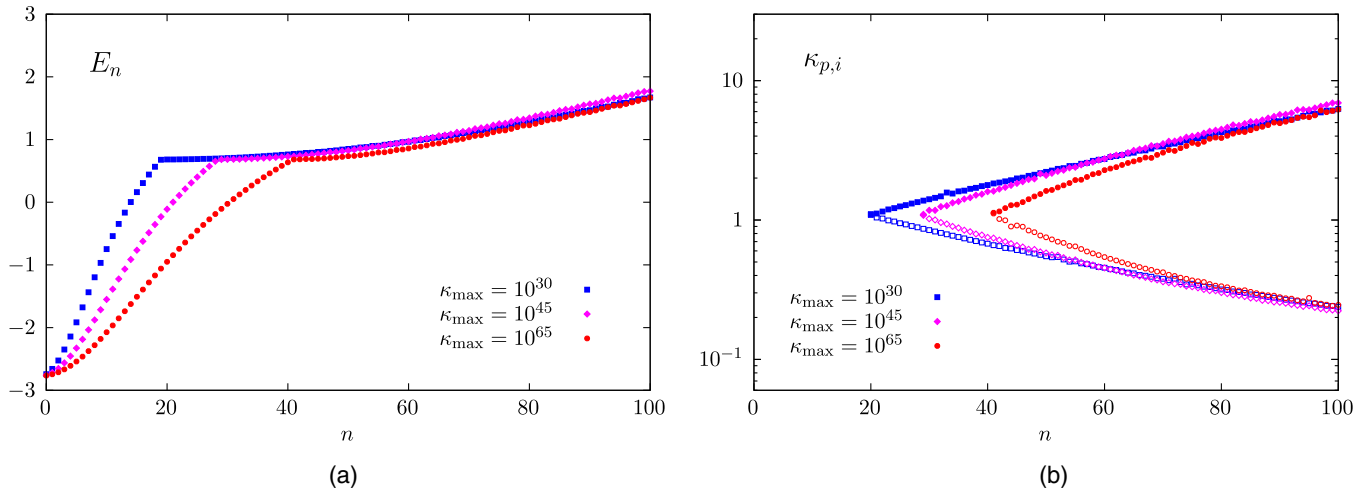

FIG. 15. The eigenvalues for the Gribov gluon propagator [see Eq. (11e) with $m = 0$ and $m_0 = 0$] vs n [Fig. 15(a)]. The value of n at which energy E_n reaches E_0 can be found from the equation $\beta_n = \beta^0 = 0.85$. Figure 15(b) shows the dependence of two poles in Eq. (59) on n at different values of $\kappa_{\max}$. Note that the minimal value of n when two poles $\kappa_{p,i}$ appear is determined by the same condition $\beta_n = \beta^0 = 0.85$.

with $\beta_n \propto n$ for both Gribov's and lattice QCD gluon propagators, as seen from Fig. 9(b). One can see from Fig. 5(a), that, for $\kappa \gg 1$, E_n tends to the same asymptotic values for all four equations that we have studied in this paper. For $\kappa < 1$, the eigenfunctions have the similar structure as for $E_n = E_0$; i.e., they have one pole [see Fig. 13(a)] for the lattice gluon propagator and two poles for the Gribov one [see Fig. 15(b)]. Since these eigenvalues correspond to the Pomeron intercept $\omega_{IP} = -\bar{\alpha}_S E_n < \omega_0 = -\bar{\alpha}_S E_0 < 0$, they do not contribute to the high energy behavior of the scattering amplitude.

V. SCATTERING AMPLITUDE

A. Green's function of the BFKL Pomeron for the Gribov-Zwanziger confinement

The Green's function of the BFKL equation on $Y = \ln(1/x)$ representation takes the general form

$$G(Y,\kappa_{\rm fin}|0,\kappa_{\rm in}) = \sum_{n=0}^{\infty}\int_{\epsilon-i\infty}^{\epsilon+i\infty}\frac{d\omega}{2\pi i}\frac{1}{\omega-\omega_n}e^{\omega Y}\phi_n(\kappa_{\rm in})\phi_n(\kappa_{\rm fin}) = \sum_{n=0}^{\infty}e^{-\bar{\alpha}_S E_n Y}\phi_n(\kappa_{\rm in})\phi_n(\kappa_{\rm fin}). \quad (61)$$

At high energies, the main contribution stems from the minimal energy. However, we cannot restrict ourselves by calculating only one term in Eq. (61). To demonstrate this, we use Eq. (52) for the approximate eigenfunctions, which can be written in the form

$$\phi_n^{\rm approx} = \Phi_n(\kappa)\sin\left(a_\beta(n+1)Ln(\kappa)+\varphi_n\right), \quad (62)$$

where

$$\Phi_n(\kappa) = \frac{\alpha_n(\kappa+m)}{\sqrt{(\kappa+a_n)^3}}. \quad (63)$$

The eigenvalues of Eq. (47) we calculate in diffusion approximation in which

$$\omega(n) = -\bar{\alpha}_S E_n = \omega_{\rm BFKL} - Da_\beta^2 n^2 + \mathcal{O}(n^3) = \omega_{\rm BFKL} - D\beta^2, \quad (64)$$

where $\omega_{\rm BFKL} = 4\ln 2\bar{\alpha}_S$; $D = 14\zeta(3)\bar{\alpha}_S$. Therefore, in this approximation, the Green's function takes the form

$$G(Y,\kappa_{\rm fin}|0,\kappa_{\rm in}) = e^{\omega_{\rm BFKL}Y}\sum_{n=0}^{\infty}\phi_n(\kappa_{\rm fin})\phi_n(\kappa_{\rm in})e^{-DYa_\beta^2 n^2} \to e^{\omega_{\rm BFKL}Y}\int_0^\infty d\beta\phi(\kappa_{\rm fin},\beta)\phi(\kappa_{\rm in},\beta)e^{-DY\beta^2}. \quad (65)$$

Taking the integral over β in Eq. (65), we obtain the following Green's function at large values of Y:

$$G(Y,\kappa_{\rm fin}|0,\kappa_{\rm in}) = \Phi_0(\kappa_{\rm fin})\Phi_0(\kappa_{\rm in})\frac{1}{2}e^{\omega_{\rm BFKL}Y}\sqrt{\frac{\pi}{DY}} \times\left\{e^{-\frac{(Ln(\kappa_{\rm fin})-Ln(\kappa_{\rm in}))^2}{4Da_\beta^2 Y}} - e^{-\frac{(Ln(\kappa_{\rm fin})+Ln(\kappa_{\rm in})+2a_\phi)^2}{4Da_\beta^2 Y}}\right\}. \quad (66)$$

One can see that, at large Y, $G(Y,\kappa_{\rm fin}|0,\kappa_{\rm in}) \propto (DY)^{-3/2}e^{\omega_{\rm BFKL}Y}$, which should be compared with the massless BFKL case for which $G(Y,\kappa_{\rm fin}|0,\kappa_{\rm in}) \propto (DY)^{-1/2}e^{\omega_{\rm BFKL}Y}$.

These estimates show that we need to sum the contributions of the eigenvalues in the vicinity of $n=0$. The source of such a contribution can be seen from the first two components of the sum over n in Eq. (61), which can be rewritten as

$$G(Y,\kappa_{\rm fin}|0,\kappa_{\rm in}) \propto \Phi_0(\kappa_{\rm fin})\Phi_0(\kappa_{\rm in})e^{\omega_{\rm BFKL}Y} \times\left(1+\frac{\Phi_1(\kappa_{\rm fin})\Phi_1(\kappa_{\rm in})}{\Phi_0(\kappa_{\rm fin})\Phi_0(\kappa_{\rm in})}e^{\Delta\omega_1 Y}\right), \quad (67)$$

where $\Delta\omega_1 = -\bar{\alpha}_S(E_0 - E_1)$.

For $\kappa_{\rm max}\to\infty$ $\Delta\omega_1 \to 0$, however, the product $\Delta\omega_1 Y$ at large $\kappa_{\rm max}$ and Y is undefined. Hence, we have to perform numerical estimates for the sum of Eq. (61) to determine the answer. We will discuss such a kind of estimate below. At the moment, we wish to emphasize that, since in the vicinity of $n=0$ the spectrum of the master equation coincides with the QCD BFKL equation, one can see that the influence on the asymptotic behavior of the scattering amplitude due to Gribov-Zwanziger confinement is rather small. Indeed, as we have seen from the above estimates, we obtain extra suppression of the scattering of the order of $1/(DY)$ for our case.

B. Transverse momentum distribution in the BFKL Pomeron for the Gribov-Zwanziger confinement

Using Eq. (61), we can find the scattering amplitude, which will be equal to

$$N(Y;\kappa) = \sum_{n=0}^{\infty}c_n e^{-\bar{\alpha}_S E_n Y}\phi_n(\kappa), \quad \text{with} \quad c_n = \int d\kappa_{\rm in}\phi_n(\kappa_{\rm in})N(Y=0,k_{\rm in}), \quad (68)$$

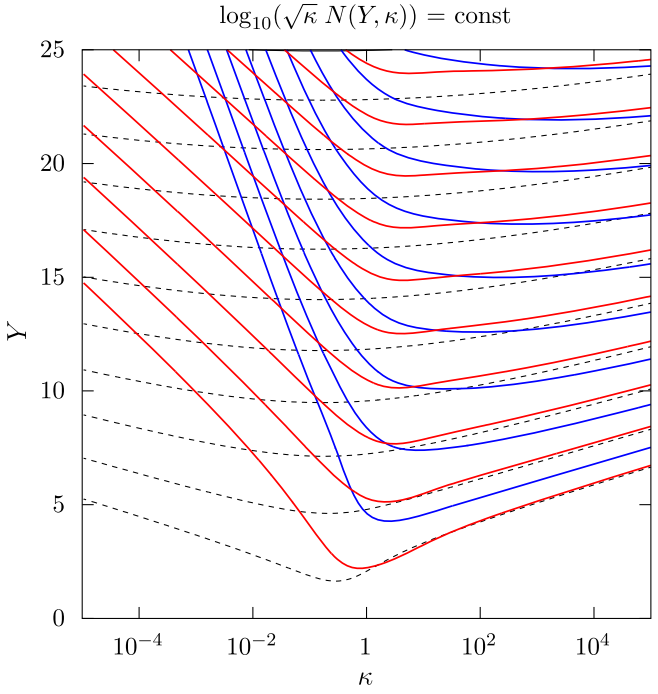

FIG. 16. The contour with constant $\kappa N(Y,\kappa)$ (see dashed line) for the QCD BFKL equation and for the BFKL equation for Gribov-Zwanziger confinement: the blue curve is for $m=0$, and the red one is for $m>0$.

where $N(Y=0,\kappa_{\rm in})$ is the initial condition for the scattering amplitude at $Y=0$. In Fig. 16, $N(Y=0,\kappa_{\rm in})$ is taken to be equal to $1/(\kappa+1)^2$. We plot in Fig. 16 the contours on which function $\kappa N(Y,\kappa)$ [see Eq. (68)] is constant. In QCD, we have transverse momentum distribution, which depends on $|\ln\kappa|$. The QCD evolution results in the increase of $|\ln\kappa|$ with Y. Such an increase leads to two possible branches (depending on different sign of $\ln\kappa$) with increasing and decreasing average transverse momentum. Such behavior is seen in Fig. 16.

For our master equation, one can see that the confinement cuts the small transverse momenta and the average κ_T are larger than the values of κ_T in initial conditions, which we consider $\kappa_{\rm in}=1$, and they grow with Y. Therefore, introducing the Gribov-Zwanziger confinement in the framework of the BFKL equation, we obtain the transverse momentum distribution, which is determined by the behavior of the scattering amplitude at large transverse momenta (at short distances), where we can trust the perturbative QCD approach.

VI. CONCLUSIONS

In this paper, we solved the new evolution equation for high energy scattering amplitude that stems from the Gribov-Zwanziger approach to the confinement of quarks and gluons [see Eq. (10a)]. We find the results of this solution quite surprising and instructive for future development of high energy physics.

First, the energy dependence of the scattering amplitude turns out to be the same as for QCD BFKL evolution. In particular, the eigenvalues of the new equation, which exceed $\omega_0=-\bar{\alpha}_S E_0=-\bar{\alpha}_S T(\kappa=0)$, coincide with the QCD BFKL equation. Second, the spectrum of the new equation does not depend on the details of the Gribov-Zwanzinger approach and coincides with the set of the eigenvalues of the model: non-Abelian gauge theories with the Higgs mechanism for mass generation, developed in Ref. [22]. This model has no relation to a QCD approach except having the same color structure. These features support the ideas that come out of the analytical analysis of the equation: the main influence of the confinement is in taking off the double degeneration of the QCD BFKL equation, which shows up in independence of the spectrum of the QCD BFKL equation on the sign of ν [see Eq. (14)]. Third, all eigenfunctions coincide with the eigenfunctions of the QCD BFKL equation at large transverse momenta $\kappa\geq 1$.

The numerical estimates show that there exist no new eigenvalues with the eigenfunctions that decreases faster than the eigenfunction of the QCD BFKL equation at large transverse momenta. The eigenfunctions of the master equation with the Gribov gluon propagator tends to zero at small transverse momenta. In the coordinate representation, it means that the eigenfunctions exhibit the powerlike decrease at long distances, leading to the powerlike decrease in the impact parameters and therefore to the severe problem with Froissart theorem and s-channel unitarity (see Refs. [3,4,27]). In other words, the gluon propagator, which tends to zero as the Gribov's propagator does, cannot solve the problem with large-b dependence of the scattering amplitude in the color glass condensate approach. However, the structure of the gluon propagator in the Gribov-Zwanziger approach that stems from the lattice QCD estimates and from the theoretical evaluation (see Refs. [43–59]) leads to the gluon propagator which tends to a finite value at zero transverse momentum $[G(q\to 0)\neq 0]$. This results in the exponential suppression of the eigenfunction at long distances and in the resolution of the difficulties that the CGC approach and other approaches, based on perturbative QCD, face at large impact parameters.

For the intercept $\omega=-\bar{\alpha}_S T(\kappa=0)$, we have the multiple degeneration of this eigenvalue, which is strongly correlated with the new dimensional parameter that we introduced to the theory from the confinement. This degeneration looks like Bose-Einstein condensation, but it does not contribute to the scattering amplitude at high energy.

We calculated the momentum distributions of the scattering amplitude and found that the typical transverse momentum increases with energy and becomes independent of the typical confinement scales that we have introduced in our equation. Therefore, to our surprise, we have to conclude that the confinement of quark and gluons, at least in the form of the Gribov-Zwanziger approach, does not influence the scattering amplitude except for solving the long-standing theoretical problem of the large impact parameter behavior of the scattering amplitude. This is a very optimistic message for the color glass condensate approach, but before coming to the strong conclusions, we have to check the solution to the nonlinear equation with the new kernel. This will be our next problem.

ACKNOWLEDGMENTS

We thank our colleagues at Tel Aviv University and Universidad Técnica Federico Santa María for encouraging discussions. This research was supported by Agencia Nacional de Investigación y Desarrollo Programa de Investigación Asociativa/APOYO AFB180002 (Chile) and FONDECYT (Chile) Grant No. 1180118.

[1] M. Froissart, Asymptotic behavior and subtractions in the Mandelstam representation, Phys. Rev. **123**, 1053 (1961); A. Martin, *Scattering Theory: Unitarity, Analitysity and Crossing*, Lecture Notes in Physics (Springer-Verlag, Berlin, 1969).

[2] Y. V. Kovchegov and E. Levin, *Quantum Choromodynamics at High Energies*, Cambridge Monographs on Particle Physics, Nuclear Physics and Cosmology (Cambridge University Press, Cambridge, England, 2012), and references therein.

[3] A. Kovner and U. A. Wiedemann, Nonlinear QCD evolution: Saturation without unitarization, Phys. Rev. D **66**, 051502 (2002); Perturbative saturation and the soft pomeron, Phys. Rev. D **66**, 034031 (2002); No Froissart bound from gluon saturation, Phys. Lett. B **551**, 311 (2003).

[4] E. Ferreiro, E. Iancu, K. Itakura, and L. McLerran, Froissart bound from gluon saturation, Nucl. Phys. **A710**, 373 (2002).

[5] V. S. Fadin, E. A. Kuraev, and L. N. Lipatov, On the pomeranchuk singularity in asymptotically free theories, Phys. Lett. **60B**, 50 (1975); E. A. Kuraev, L. N. Lipatov, and V. S. Fadin, The Pomeranchuk singularity in nonabelian gauge theories, Zh. Eksp. Teor. Fiz. **72**, 377 (1977) [Sov. Phys. JETP **45**, 199 (1977)]; I. I. Balitsky and L. N. Lipatov, The Pomeranchuk singularity in quantum chromodynamics, Yad. Fiz. **28**, 1597 (1978) [Sov. J. Nucl. Phys. **28**, 822 (1978)].

[6] L. N. Lipatov, The bare pomeron in quantum chromodynamics, Zh. Eksp. Teor. Fiz. **90**, 1536 (1986) [Sov. Phys. JETP **63**, 904 (1986)].

[7] E. M. Levin and M. G. Ryskin, High-energy hadron collisions in QCD, Phys. Rep. **189**, 268 (1990).

[8] E. M. Levin and M. G. Ryskin, The shrinkage of the diffraction peak of the bare pomeron in QCD, Z. Phys. C **48**, 231 (1990); Yad. Fiz. **50**, 1417 (1989) [Sov. J. Nucl. Phys. **50**, 881 (1989)].

[9] E. Levin and C. I. Tan, Heterotic Pomeron: A Unified Treatment of High-Energy Hadronic Collisions in *QCD, in Santiago de Compostela 1992, Proceedings, Multiparticle dynamics* 568-575 and Fermilab Batavia—FERMILAB-Conf-92-391 (92/09,rec.Jan.93) 9 p. 303600, Brown University Providence—BROWN-HET-889 (92/09, rec.Jan.93).

[10] D. Y. Ivanov, R. Kirschner, E. M. Levin, L. N. Lipatov, L. Szymanowski, and M. Wusthoff, The BFKL pomeron in $(2+1)$-dimensional QCD, Phys. Rev. D **58**, 074010 (1998).

[11] D. Kharzeev and E. Levin, Scale anomaly and 'soft' pomeron in QCD, Nucl. Phys. **B578**, 351 (2000).

[12] D. E. Kharzeev, Y. V. Kovchegov, and E. Levin, QCD instantons and the soft pomeron, Nucl. Phys. **A690**, 621 (2001).

[13] K. J. Golec-Biernat and A. M. Stasto, On solutions of the Balitsky-Kovchegov equation with impact parameter, Nucl. Phys. **B668**, 345 (2003).

[14] S. Bondarenko, E. Levin, and C. I. Tan, High energy amplitude as an admixture of 'soft' and 'hard' pomerons, Nucl. Phys. **A732**, 73 (2004).

[15] E. Gotsman, M. Kozlov, E. Levin, U. Maor, and E. Naftali, Towards a new global QCD analysis: Solution to the nonlinear equation at arbitrary impact parameter, Nucl. Phys. **A742**, 55 (2004).

[16] Y. Hatta and A. H. Mueller, Correlation of small-x gluons in impact parameter space, Nucl. Phys. **A789**, 285 (2007).

[17] A. H. Mueller and S. Munier, Correlations in impact-parameter space in a hierarchical saturation model for QCD at high energy, Phys. Rev. D **81**, 105014 (2010).

[18] J. Berger and A. M. Stasto, Small x nonlinear evolution with impact parameter and the structure function data, Phys. Rev. D **84**, 094022 (2011).

[19] J. Berger and A. Stasto, Numerical solution of the nonlinear evolution equation at small x with impact parameter and beyond the LL approximation, Phys. Rev. D **83**, 034015 (2011).

[20] A. Kormilitzin and E. Levin, Non-linear equation: Energy conservation and impact parameter dependence, Nucl. Phys. **A849**, 98 (2011).

[21] E. Levin and S. Tapia, BFKL Pomeron: Modeling confinement, J. High Energy Phys. 07 (2013) 183.

[22] E. Levin, L. Lipatov, and M. Siddikov, BFKL Pomeron with massive gluons, Phys. Rev. D **89**, 074002 (2014).

[23] E. Levin, Large **b** behaviour in the CGC/saturation approach: BFKL equation with pion loops, Phys. Rev. D **91**, 054007 (2015).

[24] D. E. Kharzeev and E. M. Levin, Color Confinement and Screening in the θ Vacuum of QCD, Phys. Rev. Lett. **114**, 242001 (2015).

[25] O. V. Kancheli, On the parton picture of Froissart asymptotic behavior, arXiv:1609.07657.

[26] E. Gotsman and E. Levin, Large impact parameter behavior in the CGC/saturation approach: A new nonlinear equation, Phys. Rev. D **101**, 014023 (2020).

[27] E. Gotsman and E. Levin, Gribov-Zwanziger confinement, high energy evolution and large impact parameter behaviour of the scattering amplitude, Phys. Rev. D **103**, 014020 (2021).

[28] V. N. Gribov, Quantization of nonabelian gauge theories, Nucl. Phys. **B139**, 1 (1978).

[29] V. N. Gribov, The theory of quark confinement, Eur. Phys. J. C **10**, 91 (1999).

[30] V. N. Gribov, ORSAY lectures on confinement. 1., arXiv:hep-ph/9403218.

[31] V. N. Gribov, Orsay lectures on confinement. 2., arXiv:hep-ph/9404332.

[32] V. N. Gribov, Orsay lectures on confinement (III), arXiv:hep-ph/9905285.

[33] P. van Baal, More (thoughts on) Gribov copies, Nucl. Phys. **B369**, 259 (1992).

[34] D. Zwanziger, Local and renormalizable action from the Gribov horizon, Nucl. Phys. **B323**, 513 (1989).

[35] D. Zwanziger, Vanishing of zero momentum lattice gluon propagator and color confinement, Nucl. Phys. **B364**, 127 (1991).

[36] D. Zwanziger, Renormalizability of the critical limit of lattice gauge theory by BRS invariance, Nucl. Phys. **B399**, 477 (1993).

[37] N. Vandersickel and D. Zwanziger, The Gribov problem and QCD dynamics, Phys. Rep. **520**, 175 (2012), and references therein.

[38] Y. L. Dokshitzer and D. E. Kharzeev, The Gribov conception of quantum chromodynamics, Annu. Rev. Nucl. Part. Sci. **54**, 487 (2004).

[39] D. Dudal, C. P. Felix, M. S. Guimaraes, and S. P. Sorella, Accessing the topological susceptibility via the Gribov horizon, Phys. Rev. D **96**, 074036 (2017).
[40] G. Veneziano, U(1) without instantons, Nucl. Phys. **B159**, 213 (1979).
[41] E. Witten, Current algebra theorems for the U(1) Goldstone boson, Nucl. Phys. **B156**, 269 (1979).
[42] D. Dudal, O. Oliveira, and P. J. Silva, High precision statistical Landau gauge lattice gluon propagator computation vs. the Gribov-Zwanziger approach, Ann. Phys. (Amsterdam) **397**, 351 (2018).
[43] A. Cucchieri, D. Dudal, T. Mendes, and N. Vandersickel, Modeling the gluon propagator in Landau gauge: Lattice estimates of pole masses and dimension-two condensates, Phys. Rev. D **85**, 094513 (2012).
[44] D. Dudal, O. Oliveira, and N. Vandersickel, Indirect lattice evidence for the Refined Gribov-Zwanziger formalism and the gluon condensate $\langle A^2 \rangle$ in the Landau gauge, Phys. Rev. D **81**, 074505 (2010).
[45] M. Q. Huber, Nonperturbative properties of Yang–Mills theories, Phys. Rep. **879**, 1 (2020).
[46] M. A. L. Capri, D. Fiorentini, A. D. Pereira, and S. P. Sorella, Renormalizability of the refined Gribov-Zwanziger action in linear covariant gauges, Phys. Rev. D **96**, 054022 (2017).
[47] A. K. Cyrol, L. Fister, M. Mitter, J. M. Pawlowski, and N. Strodthoff, Landau gauge Yang-Mills correlation functions, Phys. Rev. D **94**, 054005 (2016).
[48] D. Dudal, S. P. Sorella, and N. Vandersickel, The dynamical origin of the refinement of the Gribov-Zwanziger theory, Phys. Rev. D **84**, 065039 (2011).
[49] M. Q. Huber, R. Alkofer, and S. P. Sorella, Non-perturbative analysis of the Gribov-Zwanziger action, AIP Conf. Proc. **1343**, 158 (2011).
[50] M. Q. Huber, R. Alkofer, and S. P. Sorella, Non-perturbative analysis of the Gribov-Zwanziger action, AIP Conf. Proc. **1343**, 158 (2011).
[51] R. Alkofer, M. Q. Huber, and K. Schwenzer, Infrared singularities in Landau gauge Yang-Mills theory, Phys. Rev. D **81**, 105010 (2010).
[52] J. A. Gracey, Alternative refined Gribov-Zwanziger Lagrangian, Phys. Rev. D **82**, 085032 (2010).
[53] C. S. Fischer, A. Maas, and J. M. Pawlowski, On the infrared behavior of Landau gauge Yang-Mills theory, Ann. Phys. (Amsterdam) **324**, 2408 (2009).
[54] D. Dudal, S. P. Sorella, N. Vandersickel, and H. Verschelde, New features of the gluon and ghost propagator in the infrared region from the Gribov-Zwanziger approach, Phys. Rev. D **77**, 071501 (2008).
[55] D. Dudal, J. A. Gracey, S. P. Sorella, N. Vandersickel, and H. Verschelde, A refinement of the Gribov-Zwanziger approach in the Landau gauge: Infrared propagators in harmony with the lattice results, Phys. Rev. D **78**, 065047 (2008).
[56] M. A. L. Capri, V. E. R. Lemes, R. F. Sobreiro, S. P. Sorella, and R. Thibes, The influence of the Gribov copies on the gluon and ghost propagators in Euclidean Yang-Mills theory in the maximal Abelian gauge, Phys. Rev. D **72**, 085021 (2005).
[57] D. Zwanziger, Nonperturbative Faddeev-Popov formula and infrared limit of QCD, Phys. Rev. D **69**, 016002 (2004).
[58] D. Zwanziger, Nonperturbative Landau gauge and infrared critical exponents in QCD, Phys. Rev. D **65**, 094039 (2002).
[59] C. Lerche and L. von Smekal, On the infrared exponent for gluon and ghost propagation in Landau gauge QCD, Phys. Rev. D **65**, 125006 (2002).
[60] I. Gradstein and I. Ryzhik, *Table of Integrals, Series, and Products*, 5th ed. (Academic Press, London, 1994).